A HLLC scheme for nonconservative hyperbolic problems. Application to turbidity currents with sediment transport

M.J. Castro Díaz [*], E.D. Fernández-Nieto, [†], T. Morales de Luna [‡], G. Narbona-Reina [§], C. Parés [¶]

Abstract

This paper focuses on the generalization of the HLLC Riemann solver for nonconservative problems. First, the general ideas of the extension of the HLLC solvers for nonconservative systems are discussed. Then, two particular HLLC solvers are described for a turbidity current model with sediment transport. Some results concerning the positivity of the corresponding schemes are presented. Several numerical tests are performed to compare the two HLLC solvers among them and with a Roe method.

keywords: Well-balanced, Finite Volume Method, path-conservative, simple Riemann solver, HLLC.

1 Introduction

The goal of this paper is to extend to nonconservative hyperbolic systems HLLC Riemann solver. HLL solver was introduced by Harten, Lax, and van Leer in [11] in the framework of systems of conservation laws. The main idea of this solver is to approximate exact solutions of Riemann problems by a simplified solution consisting in two waves speeds which separate three constant states. This incomplete

[*]Departamento de Análisis Matemático, Universidad de Málaga. F. Matemáticas, Campus Teatinos S/N, Spain (castro@anamat.cie.uma.es)

[†]Departamento de Matemática Aplicada I, Universidad de Sevilla. E.T.S. Arquitectura. Avda, Reina Mercedes, s/n. 41012 Sevilla, Spain (edofer@us.es)

[‡]Dpto. de Matemáticas. Universidad de Córdoba. Campus de Rabanales. 14071 Córdoba (tomas.morales@uco.es)

[§]Departamento de Matemática Aplicada I, Universidad de Sevilla. E.T.S. Arquitectura. Avda, Reina Mercedes, s/n. 41012 Sevilla, Spain (gnarbona@us.es)

[¶]Departamento de Análisis Matemático, Universidad de Málaga. F. Matemáticas, Campus Teatinos S/N, Spain (pares@anamat.cie.uma.es)

Riemann solver is the basis of many efficient and robust Godunov-type schemes. Nevertheless, for systems with three or more equations, the assumption of a two-wave configuration may lead to inaccurate resolution of some physical features such as contact discontinuities, shear waves, etc. This motivated the introduction of HLLC Riemann solver (where C stands for Contact) by Toro, Spruce, and Speares in [26]. HLLC solver introduces one or more intermediate waves to the structure of the approximate solutions of the Riemann problem, improving thus the accuracy of the scheme.

In [21], the concept of approximate Riemann solvers was generalized to nonconservative systems and provides a suitable framework to extend incomplete Riemann solvers and in particular HLLC scheme. This framework is based on the definition of weak solutions by Dalmaso, LeFloch and Murat in [8] and will allows us to define a HLLC scheme for the particular P.D.E. system that models turbidity currents. Besides its practical interest, this model may be considered as a prototype of hyperbolic systems with nonconservative products and source terms and the main ideas can be easily extended.

The system for turbidity currents presented here was introduced in [18] where a path-conservative Roe scheme was proposed for numerical simulations. It is well known that Roe solvers define an approximate solution of Riemann problems composed by a number of waves equals to the number of equations. Roe scheme is what we call a complete Riemann solver as all the intermediate waves are taken into account and it needs an explicit knowledge of the eigenstructure of the system. This makes Roe scheme to be an expensive scheme from the computational point of view and a less expensive and accurate scheme is desired.

The major difficulty in numerical discretization of nonconservative systems is that the formal consistency with a particular definition of weak solutions does not imply that the limits of the numerical approximations are weak solutions according to the prescribed definition: this difficulty, that also appears when nonconservative numerical schemes are applied to systems of conservation laws (see [12]), has been studied in [5]. Another example of this phenomenon has been shown in [1]. In practice, this difficulty, which is related to numerical viscosity of the scheme, may be observed in the presence of shocks in numerical solutions that do not satisfy the prescribed jump conditions for the definition of weak solutions (see [23] for further details). Nevertheless, the error committed in shocks may be small compared to discretization or modeling errors and is only relevant in presence of large shocks.

This paper is organized as follows: in Section 2 we present the general equations of the turbidity currents model. In Section 3, some preliminary definitions are introduced with focus in approximate Riemann solvers.

In Section 4 HLLC solvers are introduced in a general framework which will be used to derive a HLLC solver for turbidity currents in Section 5. Two types of HLLC solvers will be presented. The first one, to which is devoted most of Section 5, will be called *essentially three wave HLLC solver* (E3W-HLLC). The second one, which is only briefly described here, will be called a *four wave HLLC solver* (4W-

HLLC). While the second one is more complex and general than the first one, we will see that numerical simulations obtained with it are only slightly improved. The positivity-preserving properties of the corresponding numerical schemes as well as their relationship with the Suliciu relaxation method for the shallow water system studied in [3] will be analyzed.

Finally, some numerical tests are presented in Section 6 to validate the numerical schemes, and comparison with Roe's method introduced in [18] are provided. A study of above mentioned difficulties on convergence for discontinuous solutions will also be made.

2 Turbidity current model

When a river that flows into the sea carries a high concentration of suspended sediment, to the extent that the density of the river is greater than that of the receiving ambient water, the river plunges into the ocean creating what we call a turbidity current or hyperpycnal plume. This plume can travel significant distances until it loses its identity by entraining surrounding ambient water and dropping its sediment load. In [18] a new model for the simulation of turbidity currents was introduced. This model can be described as follows: let us consider $n_s \geq 1$ species of sediments with constant density ρ_j, for $j = 1, \ldots, n_s$ transported by a river with freshwater of constant density ρ_0. The river flows in an ambient fluid (in general the sea) of density ρ_w.

The governing equations for the dilute turbidity current are as follows:

$$\begin{cases} \partial_t h + \nabla_x \cdot (h\vec{u}) = \phi_\eta + \phi_b, \\ \partial_t (h\vec{u}) + \nabla_x \cdot (h\vec{u} \otimes \vec{u}) + \nabla_x \left(g\,(R_0 + R_c)\,\dfrac{h^2}{2} \right) = -g\,(R_0 + R_c)\,h \nabla_x (z_b - H) + \\ \qquad\qquad + \vec{u}\phi_\eta + \dfrac{\vec{u}}{2}\phi_b, \\ \partial_t (hc_j) + \nabla_x \cdot (hc_j\vec{u}) = \phi_b^j, \text{ for } j = 1, \ldots, n_s, \\ \partial_t z_b + \nabla_x q_b = -\xi \phi_b, \end{cases} \tag{2.1}$$

where h is the thickness of the plume; $\vec{u}$ is the depth-averaged horizontal velocity; c_j for $j = 1, \ldots, n_s$ represents the vertically averaged volume concentration of the jth sediment specie; $c = \sum_{i=1}^{n_s} c_j$, is the total sediment concentration; and

$$R_j = \frac{\rho_j - \rho_0}{\rho_0}, \text{ for } j = 1, \ldots, n_s; \quad R_0 = \frac{\rho_0 - \rho_w}{\rho_0}; \quad \text{and } R_c = \sum_{j=1}^{n_s} R_j c_j. \tag{2.2}$$

We will denote by $\vec{q} = h\vec{u}$ the water discharge.

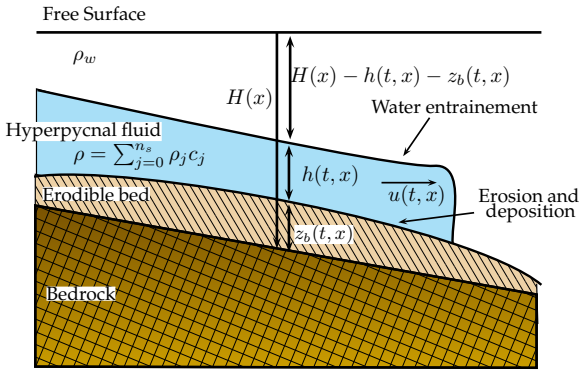

Figure 1: Sketch of a turbidity current.

Remark 2.1 *When the ambient fluid is the sea the approximation* $\rho_0 \approx \rho_w$ *may be considered and thus* $R_0 = 0$. *When the ambient fluid is the air, the approximation* $\rho_w \approx 0$ *may be taken and thus* $R_0 = 1$.

$z_b - H$ is the interface between the bottom and the fluid. z_b is the thickness of the sediment layer which may be modified by the fluid by erosion, deposition or bedload transport. H is the depth from the surface where the non-erodible bottom is located (see Fig. 1). Finally, $q_b = q_b(h, \vec{u}, c, z_b)$ represents the solid transport discharge, which is usually given by an empirical formula. Many different expressions of this formula have been proposed in the literature. Among the simplest ones we find the formula proposed by Grass [10]:

$$q_b(\vec{u}) = \xi A |\vec{u}|^{m-1} \vec{u}, \tag{2.3}$$

where A is the constant of interaction between the fluid and the sediment layer, ξ is related to the porosity $p \in [0, 1]$ by $\xi = \frac{1}{1-p}$, and m is a parameter which is usually set to $m = 3$. We refer to [6] and [18] and the references therein for details about some other possible expressions for q_b.

Fowler proposes in [9] (see also [17]) a new expression of q_b that depends not only on the flow variables, as it is the case in (2.3) but also on the thickness of the sediment layer. This dependence is in agreement with the physics of the problem: if $z_b = 0$, the sediment transport flux has to be 0, which is not the case for the Grass model. Therefore, we will consider here the following modified Grass solid transport discharge:

$$q_b = \xi \frac{z_b}{\bar{z}} A |\vec{u}|^{m-1} \vec{u},$$

where $\bar{z}$ is a mean value of the thickness of the sediment layer.

In what follows, we shall consider this modification for solid transport discharge and denote by

$$q_b = z_b \tilde{q}_b(h, \vec{u}, c) \tag{2.4}$$

where

$$\tilde{q}_b(h,u,c) = \xi \frac{A}{\bar{z}} |\vec{u}|^{m-1} \vec{u}. \tag{2.5}$$

Nevertheless, everything that will be said and in particular Section 5 remains valid if we use any of the well-known classical formulae for $\tilde{q}_b$.

The source terms ϕ_η and ϕ_b^j represent respectively the amount of sea water entrained and mixed by turbulence to the plume, and the deposition/erosion flux of the jth sediment specie. These source terms are given by different empirical laws which depend on the physical properties of the sediment. In general, water entrainment is described as

$$\phi_\eta = E_w |\vec{u}|, \tag{2.6}$$

where E_w is some function which depends on the Richardson number $\mathcal{Ri} = \dfrac{R_c g h}{|\vec{u}|^2}$.

The sediment flux at the bed of the jth specie is determined from the rates of deposition (F_d^j) and erosion (F_e^j),

$$\phi_b = \sum_{j=1}^{n_s} \phi_b^j, \quad \phi_b^j = F_e^j - F_d^j, \quad F_d^j = v_{s_j} c_{b_j}, \quad F_e^j = v_{s_j} p_j E_{s_j}, \tag{2.7}$$

where v_{s_j} is the settling velocity, c_{b_j} is the near bed concentration of sediment which may be described in terms of c_j, p_j is the volumetric concentration of sediment j in the bed and E_{s_j} is a function that usually depends on the velocity $\vec{u}$. We remark that there are some discrepancies in the mathematical expression of the source terms ϕ_η and ϕ_b^j. The expressions proposed in [24], [15], [13] and [18] are among the most used, but some variants may be found in [2], [4] and [14]. We refer to those works for further details.

Remark that system (2.1) is invariant under rotation. This rotational invariance allows us to easily define a numerical scheme for (2.1) from any given numerical scheme defined for the one-dimensional case as it is done in [???]. For the sake of simplicity and without loss of generality we shall consider the one-dimensional case with one sediment specie whose concentration is denoted by c. We also consider $R_0 = 1$ (see Remark 2.1). The PDE system reduces to:

$$\begin{cases} \partial_t h + \partial_x (hu) = \phi_\eta + \phi_b, \\ \partial_t (hu) + \partial_x \left(hu^2 + g\,(1+Rc)\,\dfrac{h^2}{2} \right) = -g\,(1+Rc)\,h \partial_x (z_b - H) + u\phi_\eta + \dfrac{u}{2}\phi_b, \\ \partial_t (hc) + \partial_x (hu\,c) = \phi^b, \\ \partial_t z_b + \partial_x q_b = -\xi \phi_b, \end{cases} \tag{2.8}$$

where $R = (\rho_1 - \rho_0)/\rho_0$. This system can be rewritten as follows:

$$\partial_t W + \partial_x F(W) + B(W)\partial_x W - S(W)\partial_x H = G(W) \tag{2.9}$$

where $W = (h, uh, hc, z_b)$, $F(W) = F_C(W) + F_P(W)$ being

$$F_C(W) = \begin{pmatrix} hu \\ hu^2 \\ huc \\ q_b \end{pmatrix}, \quad F_P(W) = \begin{pmatrix} 0 \\ \frac{1}{2}g(1+Rc)h^2 \\ 0 \\ 0 \end{pmatrix}, \tag{2.10}$$

$$B(W) = \begin{pmatrix} 0 & 0 & 0 & 0 \\ 0 & 0 & 0 & g(1+Rc)h \\ 0 & 0 & 0 & 0 \\ 0 & 0 & 0 & 0 \end{pmatrix}, \qquad S(W) = \begin{pmatrix} 0 \\ g(1+Rc)h \\ 0 \\ 0 \end{pmatrix}, \tag{2.11}$$

and

$$G(W) = \begin{pmatrix} \phi_\eta + \phi_b \\ u\phi_\eta + \dfrac{u}{2}\phi_b \\ \phi^b \\ -\xi\phi_b \end{pmatrix}. \tag{2.12}$$

Finally, system (2.9) can also be rewritten in a more compact form as follows:

$$\partial_t \begin{pmatrix} W \\ H \end{pmatrix} \left(\begin{array}{c|c} \mathcal{A}(W) & -S(W) \\ \hline 0 & 0 \end{array}\right) \partial_x \begin{pmatrix} W \\ H \end{pmatrix} = \begin{pmatrix} G(W) \\ 0 \end{pmatrix}, \tag{2.13}$$

with $\mathcal{A}(W) = J(W) + B(W)$, where $J(W) = \partial_W F(W)$ represents the Jacobian matrix of the flux function $F(W)$.

In [18] it was shown that system (2.8) is hyperbolic under some hypothesis on the solid flux q_b. Although it is not strictly hyperbolic one can always find a complete set of eigenvectors for the system. Moreover, it can be shown that the eigenvalues of the system are u with multiplicity equal to the number of sediment species plus three eigenvalues: two external eigenvalues S_L, S_R, that may be approximated by $u - \sqrt{g(1+R_c)h}$, $u + \sqrt{g(1+R_c)h}$ plus a small eigenvalue $S_M \approx 0$. The eigenvalue S_M is usually associated with the propagation of disturbances of the bed, while S_L and S_R are identified with the surface-wave celerities for a fixed-bed flow. Nevertheless, this is a rather simplified point of view only valid for small interactions between the fluid and the bed as well as small Froude number. In general, surface waves move in tandem with the bed waves, so that bed and surface waves interact strongly and S_L, S_R describe the propagation of both surface waves and bed waves and each of the celerities can not be identified solely with a surface wave or solely with a bed wave (see [19], [16], [7]).

As in [18], a splitting technique for erosion/deposition source terms will be used to approximate the solutions of system (2.8). At every time stage, first a finite volume method will be applied to the homogeneous system:

$$\partial_t \begin{pmatrix} W \\ H \end{pmatrix} \left(\begin{array}{c|c} \mathcal{A}(W) & -S(W) \\ \hline 0 & 0 \end{array}\right) \partial_x \begin{pmatrix} W \\ H \end{pmatrix} = 0, \tag{2.14}$$

and then the corresponding obtained approximations on the cells will be updated by solving the ODE:

$$\partial_t W = G(W). \tag{2.15}$$

Here we are interested in the numerical solution of (2.14) and we will neglect erosion and deposition effects because they do not add anything relevant to our purpose. These terms could be included by applying a forward Euler scheme for (2.15) as it is done in [18] and the references cited therein. For the sake of simplicity, we shall consider the case $H = constant$ so that system (2.14) may be written in the form

$$\partial_t W + \mathcal{A}(W)\partial_x W = 0. \tag{2.16}$$

Everything that will be said and in particular Section 5 can be easily adapted for the general case where H is not constant. Further comments on this fact will be made when needed.

As it is usual for shallow water models, the numerical scheme will be required to be exactly well-balanced for the water-at-rest solutions of (2.16). If it is assumed that $q = 0$ implies $q_b = 0$ (what is the case for the Grass formula (2.3)), these stationary solutions are given by:

$$q = 0, \quad c = constant, \quad h + z_b = constant. \tag{2.17}$$

3 Approximate Riemann solvers

Let us consider a general nonconservative system

$$\partial_t W + \mathcal{A}(W)\partial_x W = 0, \quad x \in \mathbb{R},\, t > 0, \tag{3.1}$$

where $W(x,t)$ belongs to Ω, an open convex subset of $\mathbb{R}^N$, and $W \in \Omega \mapsto \mathcal{A}(W) \in \mathcal{M}_N(\mathbb{R})$ is a smooth locally bounded map. We suppose that system (3.1) is strictly hyperbolic, that is, for each $W \in \Omega$ matrix $\mathcal{A}(W)$ has N real distinct eigenvalues $\lambda_1(W) < \ldots < \lambda_N(W)$, with associated eigenvectors $R_1(W), \ldots, R_N(W)$. We also suppose that for each $i = 1, \ldots, N$, the characteristic field $R_i(W)$ is either genuinely nonlinear or linearly degenerate.

In general, the nonconservative product $\mathcal{A}(W)\partial_x W$ does not make sense within the framework of classical distributions. The theory developed by Dal Maso, LeFloch, and Murat in [8] allows to give a sense to this nonconservative product as a Borel measure and thus a rigorous definition of weak solution for (3.1) can be given. According to this theory, the definition of weak solutions is based on the choice of a family of paths, i.e a family of Lipschitz continuous paths, $\Phi(s; W_L, W_R)$, $s \in [0,1]$, which must satisfy certain regularity and compatibility conditions, and in particular

$$\Phi(0; W_L, W_R) = W_L, \qquad \Phi(1; W_L, W_R) = W_R, \qquad \forall W_L, W_R \in \Omega, \tag{3.2}$$

and

$$\Phi(s; W, W) = W, \quad \forall s \in [0,1], W \in \Omega. \tag{3.3}$$

We shall not include here all the details of this theory and refer to [8] for further details. Let us only remark that weak solutions correspond to classical solutions where they are smooth, while across a discontinuity the following generalized generalized Rankine-Hugoniot condition should be satisfied:

$$\lambda[W] = \int_0^1 \mathcal{A}(\Phi(s; W^-, W^+)) \frac{\partial \Phi}{\partial s}(s; W^-, W^+)\, ds = 0, \tag{3.4}$$

where λ is the speed of propagation of the discontinuity, and $[W] = W^+ - W^-$ represents the jump of the solution at the discontinuity.

Remark 3.1 *For the particular case of system* (2.16)*, jump conditions* (3.4) *can be written as follows:*

$$\begin{cases} \lambda[h] = [q]; \\ \lambda[q] = \left[\dfrac{q^2}{h} + \dfrac{g}{2}(1 + Rc)h^2\right] \\ \qquad + \displaystyle\int_0^1 g(\Phi_h(s, W_L, W_R) + R\,\Phi_{hc}(s, W_L, W_R))\,(\partial_s \Phi_{z_b}(s, W_L, W_R))\, ds; \\ \lambda[hc] = [qc]; \\ \lambda[z_b] = [q_b]; \end{cases} \tag{3.5}$$

where Φ_h*,* Φ_{hc}*,* Φ_{z_b}*, and* Φ_H *represent the components of the chosen family of paths* Φ *for variables* h, hc, z_b*, and* H *respectively.*

Based on a family of paths Φ, Φ-approximate Riemann Solver for (3.1) were introduced in [21] as a generalization of the definition of approximate Riemann solver for system of conservation laws defined in [11].

A particular case of Φ-approximate Riemann solver is given by the so-called Φ*-simple Riemann solver.*

Definition 3.1 *A* Φ*-approximate Riemann solver* $\widetilde{V} : \mathbb{R} \times \Omega \times \Omega \mapsto \Omega$ *for* (3.1) *is said to be simple if there exists a finite number* $m \geq 1$ *of speeds*

$$\sigma_0 = -\infty < \sigma_1 < \ldots < \sigma_m < \sigma_{m+1} = +\infty, \tag{3.6}$$

and intermediate states

$$W_0 = W_L, W_1, \ldots, W_{m-1}, W_m = W_R \tag{3.7}$$

such that

$$\widetilde{V}(v, W_L, W_R) = W_j \quad \text{if } \sigma_j < v < \sigma_{j+1}. \tag{3.8}$$

Remark 3.2 *Notice that any Φ-approximate Riemann solver should satisfy*

$$\int_0^1 \mathcal{A}\left(\Phi(s;W_L,W_R)\right)\frac{\partial\Phi}{\partial s}(s;W_L,W_R)\,ds + \int_0^\infty \left(\widetilde{V}(v;W_L,W_R)-W_R\right)dv + \int_{-\infty}^0 \left(\widetilde{V}(v;W_L,W_R)-W_L\right)dv = 0. \quad (3.9)$$

for every $W_L, W_R \in \Omega$

In the particular case of a Φ-simple Riemann solver, (3.9) reduces to

$$\sum_{j=0}^{m-1}\sigma_{j+1}(W_{j+1}-W_j) = \int_0^1 \mathcal{A}\left(\Phi(s;W_L,W_R)\right)\frac{\partial\Phi}{\partial s}(s;W_L,W_R)\,ds \quad (3.10)$$

Remark 3.3 *In the particular case of the system* (2.16)*, we have*

$$\int_0^1 \mathcal{A}(\Phi(s,W_L,W_R)\partial_s\Phi(s,W_L,W_R)\,ds = F(W_R)-F(W_L)+\mathcal{B}(W_L,W_R),$$

where

$$\mathcal{B}(W_L,W_R) = \begin{pmatrix} 0 \\ \displaystyle\int_0^1 g(\Phi_h(s;W_L,W_R)+R\,\Phi_{hc}(s;W_L,W_R))\partial_s\Phi_{z_b}(s;W_L,W_R)ds \\ 0 \\ 0 \end{pmatrix}, \quad (3.11)$$

being Φ_h, Φ_{hc} and Φ_{z_b} the first, third and fourth components of Φ respectively. For the particular choice of the family of segments

$$\Phi(s;W_L,W_R) = W_L + s(W_R-W_L), \quad (3.12)$$

we get

$$\mathcal{B}(W_L,W_R) = \begin{pmatrix} 0 \\ g\left(\dfrac{h_L+h_R}{2}+R\dfrac{(hc)_L+(hc)_R}{2}\right)(z_{b\,R}-z_{b\,L}) \\ 0 \\ 0 \end{pmatrix}. \quad (3.13)$$

Given a Φ-simple Riemann Solver for (3.1) one can define a Godunov-type numerical scheme which is is path-conservative in the sense introduced in [21]:

$$W_i^{n+1} = W_i^n - \frac{\Delta t}{\Delta x}(D^+_{i-1/2}+D^-_{i+1/2}), \quad (3.14)$$

where

$$D^\pm_{i+1/2} = D^\pm(W_i^n, W_{i+1}^n), \quad (3.15)$$

with

$$D^-(W_L,W_R)=\begin{cases}\displaystyle\int_0^1 \mathcal{A}\left(\Phi(s;W_L,W_R)\right)\frac{\partial\Phi}{\partial s}(s;W_L,W_R)\,ds & \text{if } \sigma_m<0,\\ \displaystyle\sum_{\sigma_{j+1}<0}\sigma_{j+1}(W_{j+1}-W_j) & \text{if } \sigma_1<0<\sigma_m,\\ 0 & \text{if } \sigma_1>0.\end{cases} \tag{3.16}$$

$$D^+(W_L,W_R)=\begin{cases}0 & \text{if } \sigma_m<0,\\ \displaystyle\sum_{\sigma_{j+1}>0}\sigma_{j+1}(W_{j+1}-W_j) & \text{if } \sigma_1<0<\sigma_m,\\ \displaystyle\int_0^1 \mathcal{A}\left(\Phi(s;W_L,W_R)\right)\frac{\partial\Phi}{\partial s}(s;W_L,W_R)\,ds & \text{if } \sigma_1>0.\end{cases} \tag{3.17}$$

In order to discuss the well-balanced property of Φ-simple Riemann solvers, following [21] and [22], let us introduce the set Γ of all the integral curves γ of a linearly degenerate field of $\mathcal{A}(W)$ such that the corresponding eigenvalue vanishes on Γ. Recall the following definition:

Definition 3.2 *Given a curve $\gamma\in\Gamma$, a numerical scheme for solving* (3.1) *is said to be exactly well-balanced for γ if it preserves any stationary solution satisfying*

$$W(x)\in\gamma,\quad\forall\ x. \tag{3.18}$$

It can be easily shown that a numerical scheme based on a Φ-approximated Riemann solver $\widetilde{V}$ is exactly well-balanced for a curve $\gamma\in\Gamma$ if, and only if, given two states $W_L,W_R\in\Gamma$, the following equality hold:

$$\int_{-\infty}^0\left(\widetilde{V}(v;W_L,W_R)-W_L\right)dv \;=\; 0, \tag{3.19}$$

$$\int_0^{\infty}\left(\widetilde{V}(v;W_L,W_R)-W_R\right)dv \;=\; 0. \tag{3.20}$$

In particular, these equalities are trivially satisfied if

$$\widetilde{V}(v;W_L,W_R)=\begin{cases}W_L & \text{if } v<0,\\ W_R & \text{if } v>0.\end{cases} \tag{3.21}$$

Before concluding this section, let us discuss two important issues. The first one is related to the choice of the family of paths. Observe that the jump conditions (3.4) depend on the chosen family of paths. Therefore, the family of paths has to be chosen

so that the speed of propagation of discontinuities are in good agreement with the physics of the problem The key point is that, in general, first order hyperbolic models are obtained by neglecting some higher order terms whose effects are supposed to be small. Therefore, the admissible discontinuities should be the limits of traveling waves of the system including the neglected high order terms as they tend to 0. While in systems of conservation laws the jump conditions given by this passage to the limit are the classical Rankine-Hugoniot conditions independently of the particular form of the vanishing high order terms, this is not the case for nonconservative systems. Therefore, the family of paths to be chosen has to be such that the jump conditions (3.4) coincide with the ones given by the traveling waves of the regularized problems when passing to the limit. But the calculation of viscous profiles may be very difficult in practice. Moreover, in some models, as the one described in Section 2, some of the equations are given by empirical laws so that it is not clear what is the good regularized system to be considered.

On the other hand, its calculation requires the explicit knowledge of the Riemann invariants and the solutions of Riemann problems. But if such a family is considered, the use of approximate Riemann solvers is pointless, as the exact solutions of the Riemann problems are needed to compute the paths. Therefore we propose here to use simple family of paths as the one composed by the straight segments (3.12).

Remark 3.4 *In the particular case of* (2.16)*, the numerical schemes will be required to be well-balanced for the subset of* Γ *given by the water-at-rest curves* (2.17)*. Notice that these curves are straight lines in the space* h, q, hc, z_b*. Therefore, the family of segments* (3.12) *satisfies the property of being a parametrization of the arc linking two water-at-rest states and thus is a priori a good choice to design numerical schemes which are well-balanced for water-at-rest solutions (see [21]).*

For this choice of paths, the jump conditions (3.4) *reduce to:*

$$\begin{cases} \lambda[h] = [q]; \\ \lambda[q] = \left[\dfrac{q^2}{h} + \dfrac{g}{2}(1+Rc)h^2\right] + g\left(\dfrac{h^- + h^+}{2} + R\dfrac{(hc)^- + (hc)^+}{2}\right)\left(z_b^+ - z_b^-\right); \\ \lambda[hc] = [qc]; \\ \lambda[z_b] = [q_b]. \end{cases} \tag{3.22}$$

The second main difficulty is related to the convergence of the numerical solutions: even if the correct family of paths is chosen, the limits of the numerical solutions may be weak solutions corresponding to a definition different from the one given by the prescribed family. In fact, whenever a numerical scheme having some numerical viscosity is applied to a nonconservative system, the shocks appearing at the limits of the numerical solutions are consistent with the viscous profiles of

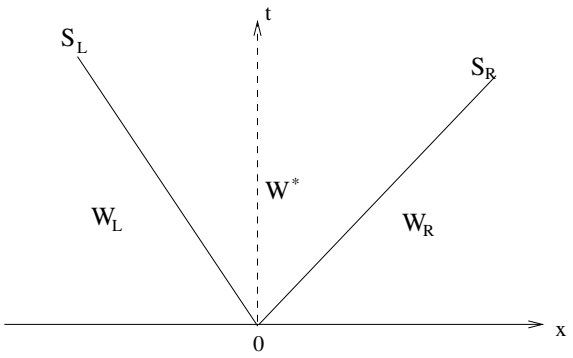

Figure 2: Control volume $[x_L, x_R] \times [0, T]$ in the $x - t$ plane

the modified equation whose viscous terms are different in general to the physical one and may lead thus to different jump conditions. Therefore, a method based on approximate or exact Riemann solvers cannot be expected to produce numerical solutions whose limits are the correct weak solutions. Nevertheless, what can be expected is to obtain stable, robust, easy-to-implement numerical methods such that:

- For system of balance laws, the limits of the numerical solutions satisfy the physical jump conditions: see [20].
- For nonconservative systems in which the nonconservative products vanish across shocks and only act in contact discontinuities, the limits of the numerical solutions also satisfy the physical jump conditions.
- For general nonconservative systems, the numerical solutions will not converge to the physical solution in general, but the convergence error is expected to be small at least for small amplitude shocks: the numerical Hugoniot curves of the states that can be linked by an entropy shock to a given state are expected to be first order approximations of the exact Hugoniot curves: see [5].

4 HLLC solver

The easiest example of Φ-simple Riemann solver for system (3.1) is HLL solver. It is a simple Riemann solver consisting of two finite-speed waves S_L, S_R linking three constant states W_L, W^*, W_R (see Fig. 2):

$$\tilde{V}^{HLL}(v; W_L, W_R) = \begin{cases} W_L & \text{if } v \leq S_L, \\ W^* & \text{if } S_L \leq v \leq S_R, \\ W_R & \text{if } v \geq S_R. \end{cases} \tag{4.1}$$

Let us suppose that a family of paths Φ has been chosen. The formal consistency condition (3.10) reduces to:

$$S_L(W^* - W_L) + S_R(W_R - W^*) = \int_0^1 \mathcal{A}\left(\Phi(s; W_L, W_R)\right) \frac{\partial \Phi}{\partial s}(s; W_L, W_R)\, ds,$$

what determines the intermediate state:

$$W^* = \frac{S_R W_R - S_L W_L - \displaystyle\int_0^1 \mathcal{A}(\Phi(s; W_L, W_R))\partial_s \Phi(s; W_L, W_R) ds}{S_R - S_L}. \tag{4.2}$$

Therefore, the HLL solver is determined once the two wave speeds S_L and S_R have been estimated. The corresponding numerical scheme is given by (3.14) - (3.17). But this solver does not satisfy the well-balanced property.

A HLLC Riemann solver is an extension of the HLL solver in which, besides the two external waves of speed ($\sigma_1 = S_L$, $\sigma_{m+1} = S_R$), $m-1$ internal waves of speed σ_2, $\ldots$, σ_m connecting m intermediate states W_1, $\ldots$, W_m are considered (see Figure 3). Therefore, it is a Φ-simple Riemann solver whose speeds and intermediate states are:

$$\sigma_0 = -\infty < S_L = \sigma_1 < \sigma_2 < \ldots \sigma_m = S_{m-1} < \sigma_{m+1} = S_R < \sigma_{m+2} = \infty, \tag{4.3}$$

$$W_0 = W_L, W_1, \ldots, W_m, W_{m+1} = W_R. \tag{4.4}$$

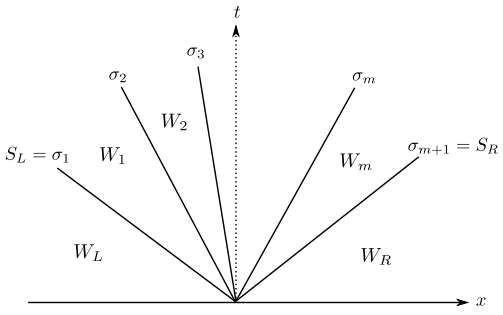

Figure 3: Sketch of a HLLC solver

If we assume that S_L and S_R are given by some estimates, then it is necessary to fix $(N+1)m - 1$ scalars to determine the simple solver: $m-1$ speeds and $N\,m$ components of the intermediate states. Notice that the N conditions given by (3.10) are enough to determine the solver only if $m = 1$, i.e. in the HLL case. For $m > 1$ some more conditions have to be taken into account in order to have the same

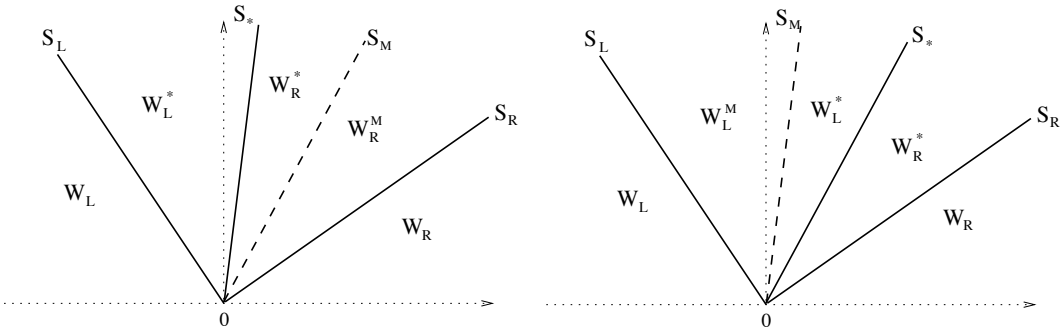

Figure 4: Waves configuration. Left: $S^* < S_M$. Right: $S_M < S^*$.

number of unknowns and equations so that the solver is determined. To do this, the jump conditions (3.4) at every intermediate wave are considered:

$$\sigma_{j+1}(W_{j+1}-W_j) = \int_0^1 \mathcal{A}(\Phi(s;W_j,W_{j+1})\partial_s\Phi(s;W_j,W_{j+1})\,ds, \quad j=0,\dots,m. \tag{4.5}$$

These jump conditions give us $(m+1)N$ more equations. In practice, at most $(N+1)m-1$ equations are chosen from the consistency condition (3.10) and the jump conditions (4.5). Let us remark that in order to have a Φ-simple solver, if some of the components of the consistency condition (3.10) are not explicitly chosen, then they should be recovered from the selected jump conditions. If the number of selected equations is lower than $(N+1)m-1$, some of the unknowns can be considered as free parameters and a family of HLLC solvers is thus obtained.

Once the intermediate speeds and states have been calculated, the corresponding numerical scheme is given by (3.14)-(3.17).

5 HLLC solver for Turbidity currents

We consider system (2.8) for turbidity currents. As we have said and for the sake of simplicity, we shall assume that $H = constant$. We do not include here erosion/deposition or water entrainment source terms, as they will be treated separately by a splitting technique.

We consider here two different HLLC solvers for the turbidity currents model using four waves of speed S_L, S_M, S^*, S_R, linking five states: $\left(W_L, W_L^M, W_L^*, W_R^*, W_R\right)$ if $S_M < S^*$ or $\left(W_L, W_L^*, W_R^*, W_R^M, W_R\right)$ if $S_M > S^*$ (see Fig. 4).

Due to the expression of the $D^{\pm}$ functions given by (3.16)-(3.17), it is enough to define the simple Riemann solver when $S_L < 0 < S_R$. Two possible configurations are then possible: $S^* < S_M$ and $S^* > S_M$. We shall denote by W_L^*, W_R^* the intermediate states to the left and to the right of the wave of speed S^* respectively. The remaining intermediate state will be denoted by W_R^M in the case $S^* < S_M$ and

W_L^M in the case $S^* > S_M$ (see Fig. 4). Remark that it is sufficient to study the case $S^* > S_M$, the other case being analogous. In order to define the solver, 14 scalars have to be fixed: the wave speeds S^*, S_M and the components of the intermediate states W_L^*, W_R^*, W_L^M. In what follows, we shall use the same indexes for each of the components of the intermediate states $W = (h, hu, hc, z_b)$.

5.1 An essentially three-wave HLLC solver

We consider the system defined by the jump conditions related to the continuity equations for the four waves speeds, and the consistency condition related to the momentum equation:

$$
\left\{
\begin{array}{ll}
(a) & \left\{
\begin{array}{rcl}
S_L(h_L^M - h_L) &=& h_L^M u_L^M - h_L u_L, \\
S_M(h_L^* - h_L^M) &=& h_L^* u_L^* - h_L^M u_L^M, \\
S^*(h_R^* - h_L^*) &=& h_R^* u_R^* - h_L^* u_L^*, \\
S_R(h_R - h_R^*) &=& h_R u_R - h_R^* u_R^*, \\
S_L(h_L^M c_L^M - h_L c_L) &=& h_L^M u_L^M c_L^M - h_L u_L c_L, \\
S_M(h_L^* c_L^* - h_L^M c_L^M) &=& h_L^* u_L^* c_L^* - h_L^M u_L^M c_L^M, \\
S^*(h_R^* c_R^* - h_L^* c_L^*) &=& h_R^* u_R^* c_R^* - h_L^* u_L^* c_L^*, \\
S_R(h_R c_R - h_R^* c_R^*) &=& h_R u_R c_R - h_R^* u_R^* c_R^*, \\
S_L(h_L^M u_L^M - h_L u_L) &+& S_M(h_L^* u_L^* - h_L^M u_L^M) \\
&+& S^*(h_R^* u_R^* - h_L^* u_L^*) + S_R(h_R u_R - h_R^* u_R^*) \\
&=& F(W_R)_{[2]} - F(W_L)_{[2]} + \mathcal{B}(W_L, W_R)_{[2]},
\end{array}
\right. \\
(b) & \left\{
\begin{array}{rcl}
S_L(z_{bL}^M - z_{bL}) &=& z_{bL}^M \tilde{q}_{bL}^M - z_{bL} \tilde{q}_{bL}, \\
S_M(z_{bL}^* - z_{bL}^M) &=& z_{bL}^* \tilde{q}_{bL}^* - z_{bL}^M \tilde{q}_{bL}^M, \\
S^*(z_{bR}^* - z_{bL}^*) &=& z_{bR}^* \tilde{q}_{bR}^* - z_{bL}^* \tilde{q}_{bL}^*, \\
S_R(z_{bR} - z_{bR}^*) &=& z_{bR} \tilde{q}_{bR} - z_{bR}^* \tilde{q}_{bR}^*,
\end{array}
\right.
\end{array}
\right. \tag{5.1}
$$

where $\tilde{q}_{bL}$, $\tilde{q}_{bL}^*$, $\tilde{q}_{bR}^*$, $\tilde{q}_{bR}$ stand for the solid transport flux $\tilde{q}_b$ evaluated in the corresponding state, the subscript $[j]$ denotes the j-th component of a vector, and $\mathcal{B}(W_L, W_R)$ is defined by (3.11). It can be easily checked that the first component of the consistency condition (3.10) is recovered by adding the first four equations, the third component is recovered by adding equations 5th to 9th, and the fourth component by adding the four last ones.

We have thus 13 equations for 14 unknowns: let us consider h_L^M as a free parameter. If the value of this parameter is fixed by:

$$h_L^M = h_L^*,$$

then a solution of system (5.1)-(a) can be found by setting $u_L^M = u_L^*$, $c_L^M = c_L^*$ and

solving then the system:

$$\left\{\begin{array}{rcl} S_L(h_L^*-h_L) &=& h_L^*u_L^*-h_Lu_L,\\ S^*(h_R^*-h_L^*) &=& h_R^*u_R^*-h_L^*u_L^*,\\ S_R(h_R-h_R^*) &=& h_Ru_R-h_R^*u_R^*,\\ S_L(h_L^*c_L^*-h_Lc_L) &=& h_L^*u_L^*c_L^*-h_Lu_Lc_L,\\ S^*(h_R^*c_R^*-h_L^*c_L^*) &=& h_R^*u_R^*c_R^*-h_L^*u_L^*c_L^*,\\ S_R(h_Rc_R-h_R^*c_R^*) &=& h_Ru_Rc_R-h_R^*u_R^*c_R^*,\\ S_L(h_L^*u_L^*-h_Lu_L) &+& S^*(h_R^*u_R^*-h_L^*u_L^*)+S_R(h_Ru_R-h_R^*u_R^*)=\\ &=& F(W_R)_{[2]}-F(W_L)_{[2]}+\mathcal{B}(W_L,W_R)_{[2]}, \end{array}\right. \tag{5.2}$$

whose solution is given by:

$$\begin{array}{rl} h_L^* &= \dfrac{h_L(S_L-u_L)}{S_L-S^*},\\ h_R^* &= \dfrac{h_R(S_R-u_R)}{S_R-S^*},\\ S^* &= \dfrac{h_Lu_L(S_L-u_L)-h_Ru_R(S_R-u_R)+\mathcal{P}_{LR}}{h_L(S_L-u_L)-h_R(S_R-u_R)},\\ u_L^* &= S^*,\\ u_R^* &= S^*,\\ c_L^* &= c_L,\\ c_R^* &= c_R, \end{array} \tag{5.3}$$

where

$$\mathcal{P}_{LR}=F_P(W_R)_{[2]}-F_P(W_L)_{[2]}+\mathcal{B}(W_L,W_R)_{[2]}.$$

If we consider some positive values k_L and k_R and define

$$\begin{array}{l} S_L=u_L-\dfrac{k_L}{h_L},\\ S_R=u_R+\dfrac{k_R}{h_R}, \end{array} \tag{5.4}$$

the solution can be written as follows:

$$\begin{array}{c} S^*=u_L^*=u_R^*=\dfrac{k_Lu_L+k_Ru_R-\mathcal{P}_{LR}}{k_L+k_R},\\ \dfrac{1}{h_L^*}=\dfrac{1}{h_L}+\dfrac{k_R(u_R-u_L)-\mathcal{P}_{LR}}{k_L(k_L+k_R)},\\ \dfrac{1}{h_R^*}=\dfrac{1}{h_R}+\dfrac{k_L(u_R-u_L)+\mathcal{P}_{LR}}{k_R(k_L+k_R)}. \end{array} \tag{5.5}$$

The subsystem (5.1)-(b) has still to be solved. Two different situations are considered:

- *Steady bottom*: If $\widetilde{q_b} = 0$, the solution is given by

$$S_M = 0, \quad z_{bL}^M = z_{bL}, \quad z_{bL}^* = z_{bR}^* = z_{bR}. \tag{5.6}$$

- *Moving bottom*: In this case, the solution is given by

$$\begin{aligned} z_{bL}^M &= \frac{u_L - \dfrac{k_L}{h_L} - \tilde{q}_{bL}}{u_L - \dfrac{k_L}{h_L} - \tilde{q}_{bL}^*} z_{bL}, \\ z_{bR}^* &= \frac{u_R + \dfrac{k_R}{h_R} - \tilde{q}_{bR}}{u_R + \dfrac{k_R}{h_R} - \tilde{q}_{bR}^*} z_{bR}, \\ z_{bL}^* &= \frac{S^* - \tilde{q}_{bR}^*}{S^* - \tilde{q}_{bL}^*} z_{bR}^*, \\ S_M &= \tilde{q}_{bL}^*. \end{aligned} \tag{5.7}$$

Remark 5.1 *Observe that:*

1. *The hydrodynamical variables are constant across the wave associated to S_M. Therefore, we have obtained a three-wave HLLC solver for the hydrodynamical variables.*

2. *In the case of non-moving bottom, the topography only jumps across the wave of speed $S_M = 0$, and nonconservative contribution is added for this wave only.*

3. *In the case of a moving bottom, S_L and S_R correspond to the external waves while S_M is the third eigenvalue that is usually associated to the motion of the bed. Remark that z_b jumps at each of the waves which is in connection to what has been said in Section 2 regarding the interaction between fluid an topography. Remark that when $\widetilde{q_b}$ is small when compared to the external wave speeds S_L, S_R, we have $z_{bL}^* \approx z_{bL}$ and $z_{bR}^* \approx z_{bR}$ which agrees with the interpretation that S_M corresponds to the motion of the sedimentary layer for small interaction between the fluid and the bed layer.*

4. *The variation of the sediment concentration c is associated to the wave S^*.*

5. *The velocities coincide at the intermediate region, $u_L^* = u_R^*$, and are equal to the intermediate wave speed S^*.*

Remark 5.2 *Note that if $R = 0$, system (2.8) coincides with the shallow-water equations with pollutant concentration.*

a) The difference between the HLLC solver proposed here and the one introduced in [25] is that in the latter the equality $h_L^* = h_R^*$ is assumed, what is not the case here.

b) If the bottom is steady and flat, the HLLC solver coincides with the Suliciu relaxation method presented in [3].

Let us introduce the following notation:

$$p(h,c) = \frac{g}{2}(1+Rc)h^2, \quad \alpha = 3/2. \tag{5.8}$$

Following the techniques introduced in [3] the following result can be proved (see Appendix A):

Theorem 5.1 *The numerical scheme based on the HLLC solver based on the definitions* (5.4) - (5.5) - (5.6) - (5.7) *with* k_L *and* k_R *given by:*

$$\text{if } \mathcal{P}_{LR} \geq 0, \quad \begin{cases} \dfrac{k_L}{h_L} = \sqrt{\dfrac{\partial p}{\partial h}(h_L, c_L)} + \alpha \left(\dfrac{\mathcal{P}_{LR}}{h_R \sqrt{\dfrac{\partial p}{\partial h}(h_R, c_R)}} + u_L - u_R \right)_+, \\ \dfrac{k_R}{h_R} = \sqrt{\dfrac{\partial p}{\partial h}(h_R, c_R)} + \alpha \left(\dfrac{-\mathcal{P}_{LR}}{k_L} + u_L - u_R \right)_+, \end{cases} \tag{5.9}$$

$$\text{if } \mathcal{P}_{LR} \leq 0, \quad \begin{cases} \dfrac{k_R}{h_R} = \sqrt{\dfrac{\partial p}{\partial h}(h_R, c_R)} + \alpha \left(\dfrac{-\mathcal{P}_{LR}}{h_L \sqrt{\dfrac{\partial p}{\partial h}(h_L, c_L)}} + u_L - u_R \right)_+, \\ \dfrac{k_L}{h_L} = \sqrt{\dfrac{\partial p}{\partial h}(h_L, c_L)} + \alpha \left(\dfrac{\mathcal{P}_{LR}}{k_R} + u_L - u_R \right)_+, \end{cases} \tag{5.10}$$

preserves the non-negativity of h.

Remark 5.3 *In the case of a moving bottom, the preservation of the non-negativity of* z_b *is not an easy task, especially for complex expressions of* $\widetilde{q}_b$. *Nevertheless, Proposition 5.2 shows that this is possible in some simple cases, for instance for Grass model, by taking large enough values of* k_L, k_R. *Remark that this is not incompatible with Theorem 5.1 as from the proof in Appendix A it follows that one could choose* k_L, k_R *arbitrarily large.*

Proposition 5.2 *Suppose that* $\widetilde{q}_b$ *only depends on the variable* u *that is, there exists some continuous function* ϕ *such that* $\tilde{q}_b(h,u,c) = \phi(u)$. *Then if* z_{bL} *and* z_{bR} *are nonnegatives, and for* $k_L, k_R > 0$ *large enough the values* $z_{b_L}^M, z_{b_L}^*, z_{b_R}^*$ *defined by (5.7) are nonnegative.*

Proof: First remark that

$$\tilde{q}_{b_L}^* = \phi(u_L^*) = \phi(u_R^*) = \tilde{q}_{b_R}^*, \tag{5.11}$$

which gives $z_{bL}^* = z_{bR}^*$.

Now, from (5.7), we have

$$z_{bL}^M = \frac{1 - \dfrac{\tilde{q}_{bL}}{u_L - k_L/h_L}}{1 - \dfrac{\tilde{q}_{bL}^*}{u_L - k_L/h_L}} z_{bL}. \tag{5.12}$$

For k_L, k_R sufficiently large, we remark that since $\tilde{q}_{bL}$ is bounded, we have

$$\frac{\tilde{q}_{bL}}{u_L - k_L/h_L} < 1. \tag{5.13}$$

We may rewrite

$$\frac{\tilde{q}_{bL}^*}{u_L - k_L/h_L} = \frac{\phi(u_L^*)}{u_L - k_L/h_L} \tag{5.14}$$

where $u_L^* = \dfrac{k_L}{k_L + k_R} u_L + \dfrac{k_R}{k_L + k_R} u_R - \dfrac{\mathcal{P}_{LR}}{k_L + k_R}$. Since $\mathcal{P}_{LR}$ does not depend on k_L and k_R, for k_L and k_R large enough, u_L^* remains bounded, and then $\phi(u_L^*)$ does too. Thus, we also obtain that

$$\frac{\tilde{q}_{bL}^*}{u_L - k_L/h_L} < 1, \tag{5.15}$$

so finally $z_{bL}^M \geq 0$.

A similar approach shows that $z_{bR}^* \geq 0$.

□

Let us check finally that HLLC solver is well-balanced for water at rest solutions. Given two states $W_L = [h_L, 0, c_L h_L, z_{b\,L}]^T$, $W_R = [h_R, 0, c_R h_R, z_{b\,R}]^T$ such that:

$$c_L = c_R = \bar{c}, \quad h_L + z_{b\,L} = h_R + z_{b\,R},$$

the following equalities can be easily checked:

$$S_M = S^* = 0, \quad W_L^M = W_L, \quad W_R^* = W_R, \quad W_L^* = [h_L, 0, \bar{c}\, h_L, z_R]^T,$$

but notice that the region in which the approximate solution takes the value W_L^* disappears. Therefore, the approximate Riemann solver reduces to (3.21) so that the numerical scheme is well-balanced.

In practice:

- the family of segments (3.12) will be used here (remember that, for this particular case, this grants well-balancing for the water-at-rest solutions (2.17));
- the speed of the fastest waves are given by (5.4) and Theorem 5.1;

- the stability requirement is $CFL \in (0,1]$, where the CFL parameter is given by:

$$CFL = \max_i \left\{ \max(\left|S_{L,i+1/2}\right|, \left|S_{R,i+1/2}\right|) \right\} \frac{\Delta t}{\Delta x}, \tag{5.16}$$

where Δx is the space step (which is assumed to be constant), Δt it the time step, and $S_{L,i+1/2}$, $S_{R,i+1/2}$ are the fastest waves considered in the approximate Riemann solver at the intercell $x_{i+1/2}$.

Remark 5.4 *If the bedrock layer is non-flat, that is $H \neq$ constant, a slight modification is needed for the HLLC solver defined before. A new wave of speed 0 has to be added where variables h, hu, hc, z_b do not jump and variable H takes the value H_L and H_R for $x < 0$ and $x > 0$ respectively. System (5.1) remains unchanged but for the 9th equation that reads now*

$$\begin{aligned} S_L(h_L^M u_L^M - h_L u_L) + S_M(h_L^* u_L^* - h_L^M u_L^M) \\ + S^*(h_R^* u_R^* - h_L^* u_L^*) + S_R(h_R u_R - h_R^* u_R^*) \\ = F(W_R)_{[2]} - F(W_L)_{[2]} + \mathcal{B}(\widetilde{W}_L, \widetilde{W}_R)_{[2]}, \end{aligned} \tag{5.17}$$

where we denote by $\widetilde{W} = (W, H)$, and

$$\mathcal{B}(\widetilde{W}_L, \widetilde{W}_R) = \begin{pmatrix} 0 \\ \displaystyle\int_0^1 g\left(\left(\Phi_h + R\,\Phi_{hc}\right)\left(\partial_s \Phi_{z_b} - \partial_s \Phi_H\right)\right)(s; \widetilde{W}_L, \widetilde{W}_R) ds \\ 0 \\ 0 \end{pmatrix}, \tag{5.18}$$

being Φ_h, Φ_{hc}, Φ_{z_b}, and Φ_H the components of the path Φ corresponding to variables h, hc, z_b, and H, respectively. This ensures that consistency condition (3.10) is satisfied.

For the particular choice of the family of segments (3.12) *we get:*

$$\mathcal{B}(\widetilde{W}_L, \widetilde{W}_R) = \begin{pmatrix} 0 \\ g\left(\dfrac{h_L + h_R}{2} + R\dfrac{(hc)_L + (hc)_R}{2}\right)(z_{b\,R} - z_{b\,L} - (H_R - H_L)) \\ 0 \\ 0 \end{pmatrix}. \tag{5.19}$$

The definition of the intermediate states (5.3) as well as the rest of the section remains the same but writing now

$$\mathcal{P}_{LR} = F_P(W_R)_{[2]} - F_P(W_L)_{[2]} + \mathcal{B}(\widetilde{W}_L, \widetilde{W}_R)_{[2]}.$$

5.2 A four-wave HLLC solver

In previous section we have defined a HLLC solver for system (2.8) based on four intermediate waves that has the property of reducing to three waves for the hydrodynamical variables. One could think on other possibilities, for instance by considering the system given by (5.1)-(a) and proposing other alternatives for (5.1)-(b). This is done in Appendix B where a four-wave HLLC solver is proposed. But as we will see in Section 6, the resulting scheme is more complex than the one proposed previously while the results obtained are only marginally better.

6 Numerical tests

We show here some test problems to compare the numerical solutions provided by the two HLLC solvers here introduced and with those provided by the Roe scheme introduced in [18]. The HLLC solvers introduced in Subsections 5.1 and 5.2 will be named hereafter as E3W-HLLC and 4W-HLLC, respectively. The family of paths considered in the definition of the three numerical schemes is the family of straight segments (3.12). If the source terms were present, a two-stage procedure would be used to update the numerical solution: once the approximations of the cell averages at the nth time level, W_i^n, have been calculated, first the HLLC or the Roe schemes are applied to the homogeneous system (2.16) to obtain the new approximations $W_i^{n+1/2}$. Then, the solutions at the $(n+1)$th time level are given by:

$$W_i^{n+1} = W_i^{n+1/2} + \Delta t G(W_i^{n+1/2}).$$

where $G(W)$ represents the source term defined by (2.12). But we focus here in the case without erosion/deposition source terms. The CFL parameter is set to 0.9.

6.1 Well-balance property

From the definitions of E3W-HLLC and 4W-HLLC it follows that both schemes are well-balanced for steady-state solutions such that

$$\begin{cases} h + z_b = Cst, \\ q = q_b = 0, \\ c = Cst. \end{cases} \tag{6.1}$$

Let us test this property numerically by considering the following initial condition

$$z_b(x,0) = 0.1e^{-(x-5.0)^2}, \quad h + z_b = 1, \quad c(x,0) = 0.05, \quad q = 0. \tag{6.2}$$

The numerical solution at $t = 1$ is computed with 100 points in the interval $[0, 5]$. The L^∞ error for both schemes is shown in Table 1.

	E3W-HLLC	4W-HLLC
h	1.514011e-12	1.513789e-12
q	1.954471e-13	1.965307e-13
z	3.246500e-13	3.246153e-13

Table 1: L^∞ error at $t = 1$ for E3W-HLLC and 4W-HLLC

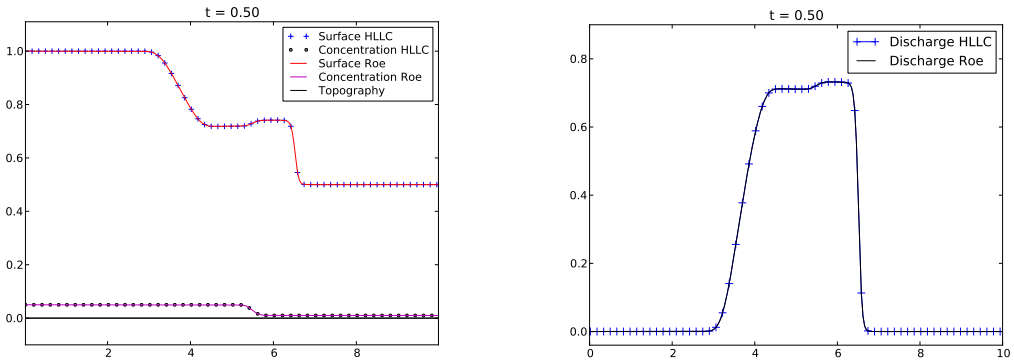

(a) (b)

Figure 5: Simulation over flat topography

6.2 Flow over a flat bottom

We consider $q_b = 0$ and $z_b = constant$. The computational domain is the interval $[0, 10]$ and the initial conditions are given by:

$$h(x,0) = \begin{cases} 1 & \text{if } x < 5, \\ 0.5 & \text{if } x \geq 5, \end{cases}, \quad c(x,0) = \begin{cases} 0.05 & \text{if } x < 5, \\ 0.01 & \text{if } x \geq 5, \end{cases} \tag{6.3}$$

and $q(x,0) = 0$ for all $x \in [0, 10]$. Free boundary conditions at both extremes of the interval are imposed by using a ghost-cell technique. In this case E3W-HLLC and 4W-HLLC coincide (see Remark B.1). The results are shown in Fig. 5.

Let us remark that E3W-HLLC and 4W-HLLC do not produce non-physical shocks so that no entropy fix is needed as it is the case for Roe scheme. For instance, consider the same test described above but now define

$$h(x,0) = \begin{cases} 2 & \text{if } x < 5, \\ 0.1 & \text{if } x \geq 5. \end{cases} \tag{6.4}$$

In this case, Roe produces a stationary shock unless an entropy fix is used as we see in Fig. 6.

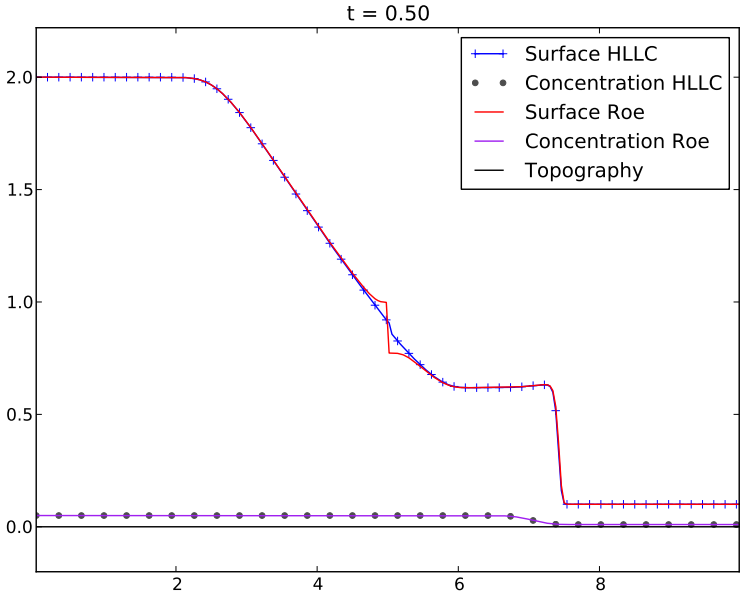

Figure 6: Entropy fix is needed for Roe scheme but not for HLLC

6.3 Transcritical flow

We consider next a transcritical flow over a bump. The equations are solved in the interval $[0, 25]$ with initial condition:

$$h(x, 0) = 0.33, \quad q(x, 0) = 0.18, \quad c(x, 0) = 0. \tag{6.5}$$

Again, $q_b = 0$ and the bottom is given by:

$$z_b(x) = \begin{cases} 0.25 - 0.05(x - 10)^2 & \text{if } 8 < x < 12, \\ 0.05 & \text{otherwise.} \end{cases} \tag{6.6}$$

The boundary conditions are $q(0, t) = 0.18$, $h(25, t) = 0.33$, and $c(0, t) = 0.02$. Fig. 7 and Fig. 8 show the steady-state reached using 250 points in the interval. Notice that the free surface and concentration (left plot in Fig. 7 and 8) computed by E3W-HLLC and 4W-HLLC are practically the same, but the computed discharge q is more accurate for the latter one (right plot in Fig. 7 and 8). We remark Roe scheme gives a better result here, specially in the zone where the shock is produced on top of the bump. This is due to the fact that Roe scheme is less diffusive than HLLC scheme but the results are comparable nonetheless.

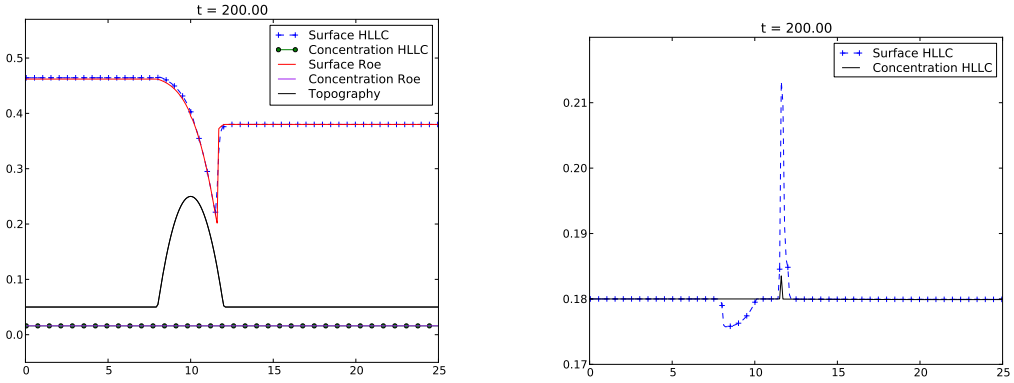

(a) (b)

Figure 7: Transcritical flow. E3W-HLLC solver

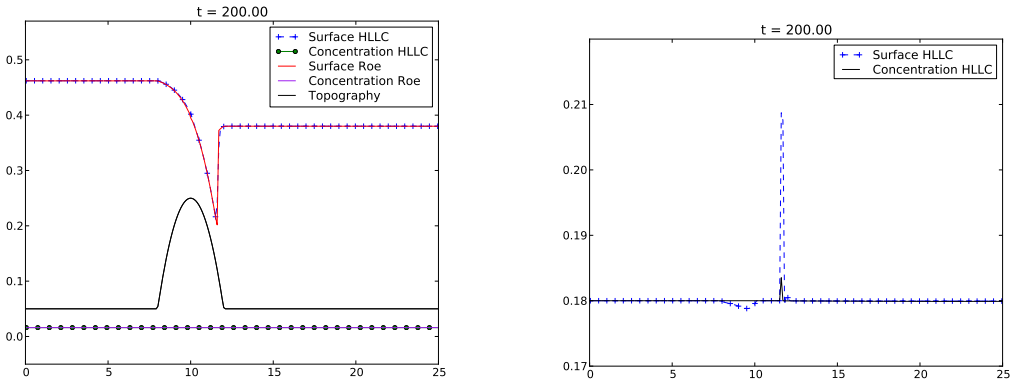

(a) (b)

Figure 8: Transcritical flow. 4W-HLLC solver

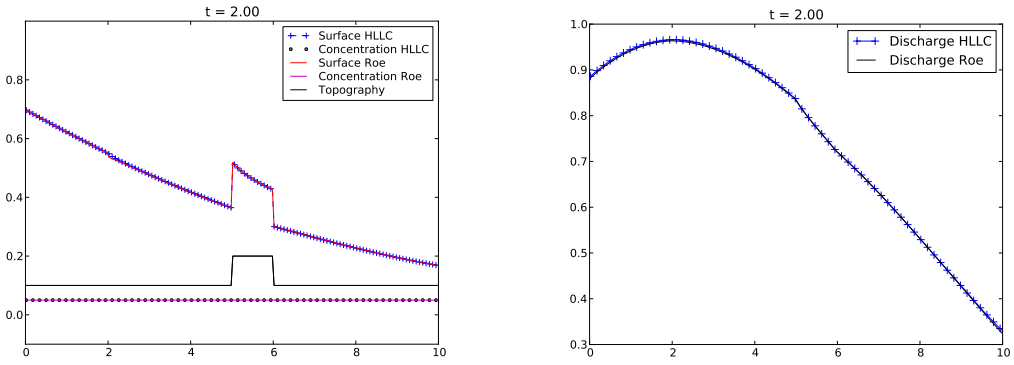

(a) (b)

Figure 9: Dam-break problem. E3W-HLLC solver

6.4 A dam-break test case

We consider next a dam-break problem over a bottom with a step. The equations are solved in the interval $[0, 10]$ with initial condition:

$$h(x,0) = \begin{cases} 1 & \text{if } x < 2, \\ 0 & \text{otherwise,} \end{cases}, \quad c(x,0) = \begin{cases} 0.05 & \text{if } x < 2, \\ 0 & \text{otherwise,} \end{cases} \tag{6.7}$$

and $q(x,0) = 0$, for all $x \in [0,10]$. We consider again $q_b = 0$ and a fixed bottom given by:

$$z_b(x) = \begin{cases} 0.2 & \text{if } 5 < x < 6, \\ 0.1 & \text{otherwise.} \end{cases} \tag{6.8}$$

Free boundary conditions are considered. The results are shown in Fig. 9 and Fig. 10 for time $t = 2$. In this test both HLLC schemes give similar results. In Fig. 11 we can observe the surface evolution for different times.

6.5 Moving bottom

In this text, the Grass solid transport formula (2.4) - (2.5) is used with $A = 0.005$. The interval is $[0, 10]$ and the initial condition is given by

$$(h+z)(x,0) = 1.1, \quad q(x,0) = 0, \quad c(x,0) = 0, \quad \forall x \in [0,10], \tag{6.9}$$

and

$$z_b(x,0) = \begin{cases} 0.2 & \text{if } 4 < x < 6, \\ 0.1 & \text{otherwise.} \end{cases} \tag{6.10}$$

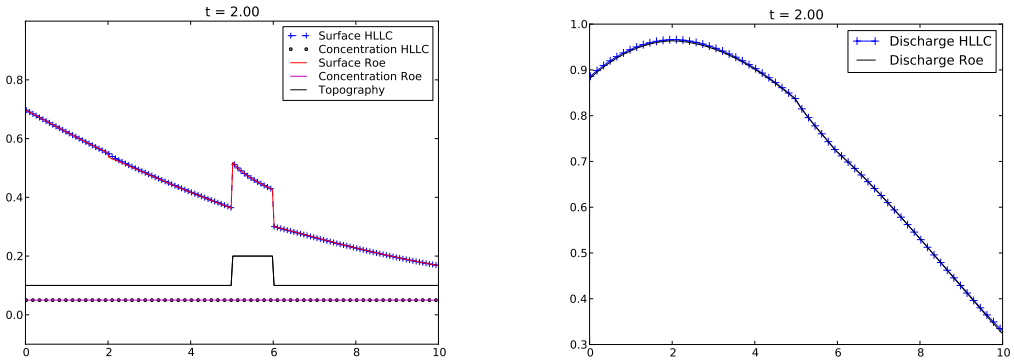

(a) (b)

Figure 10: Dam-break problem. 4W- HLLC solver

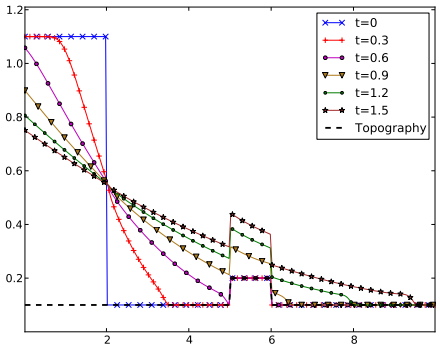

Figure 11: Surface evolution with E3W-HLLC solver

We impose the boundary conditions $q(0,t) = 0.5$ and

$$c(0,t) = \begin{cases} 0 & \text{if } t < 20, \\ 0.02(\cos(t/\pi))_+ & \text{if } t \geq 20, \end{cases} \tag{6.11}$$

so that a wave of sediments is getting into the domain periodically.

The results are shown in Fig. 12 to Fig. 16. Again the E3W-HLLC and the 4W-HLLC solvers give practically the same results for the free surface and concentration (see Fig. 12 to Fig. 15) while some differences can be observed in the discharge (see Fig. 16): again 4W-HLLC is more accurate than E3W-HLLC.

The CPU time required for this test with Roe scheme is 166.55, while with the E3W-HLLC and 4W-HLLC we need 61.57 and 65.72 respectively. This means roughly a gain 60% when using HLLC instead of Roe. Remark that E3W-HLLC is slightly faster as it does not need the computation of the intermediate velocity S_M.

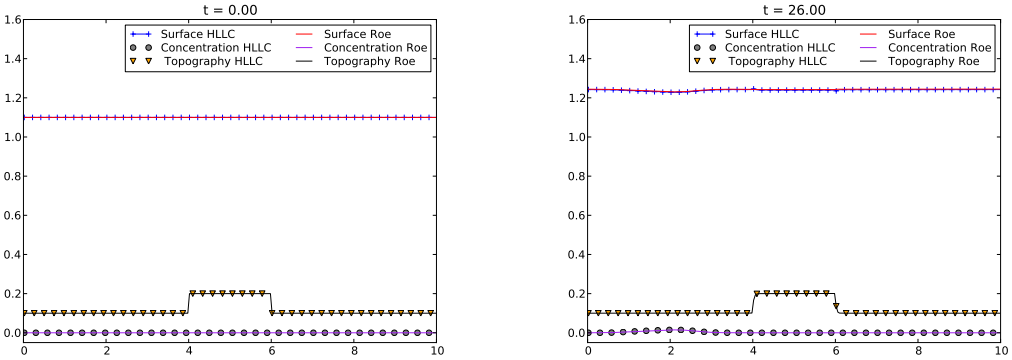

(a) (b)

Figure 12: Moving bottom: E3W-HLLC

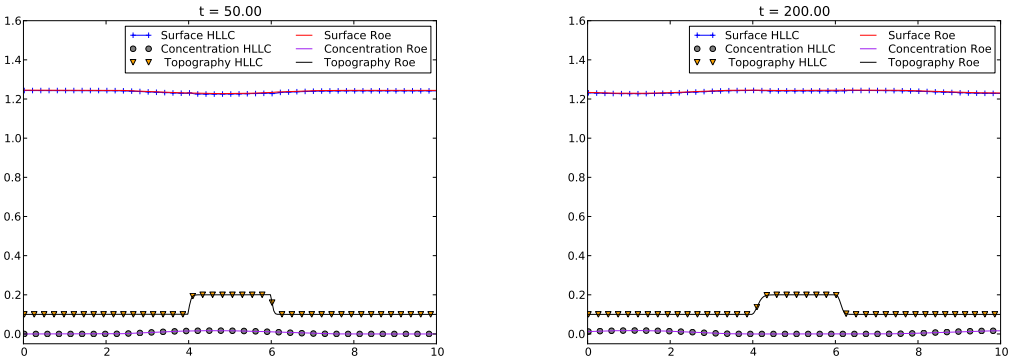

(a) (b)

Figure 13: Moving bottom: E3W-HLLC

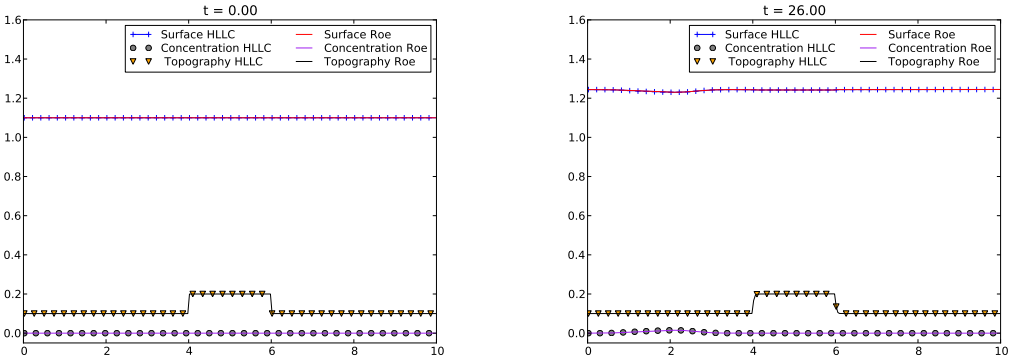

(a) (b)

Figure 14: Moving bottom: 4W-HLLC

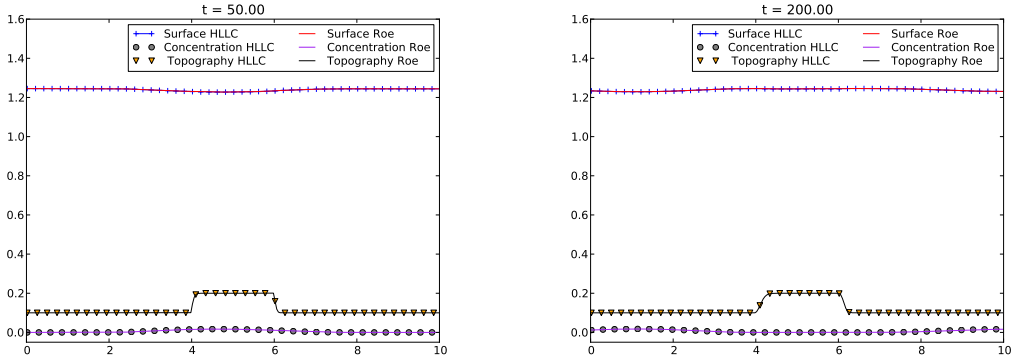

(a) (b)

Figure 15: Moving bottom: 4W-HLLC

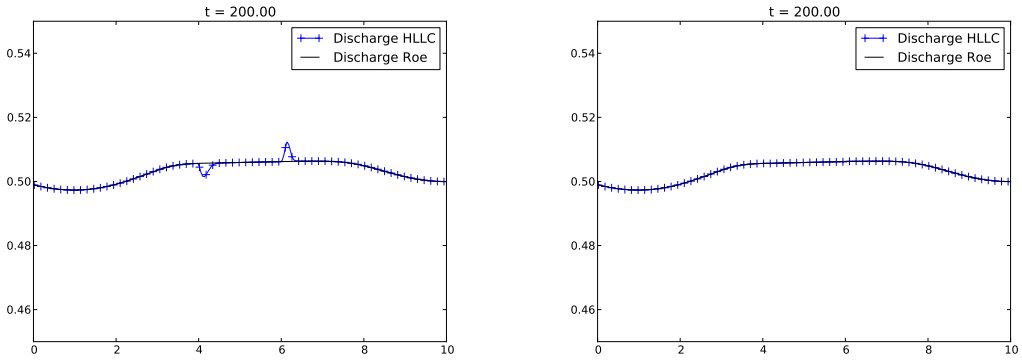

(a) E3W-HLLC (b) 4W-HLLC

Figure 16: Moving bottom.

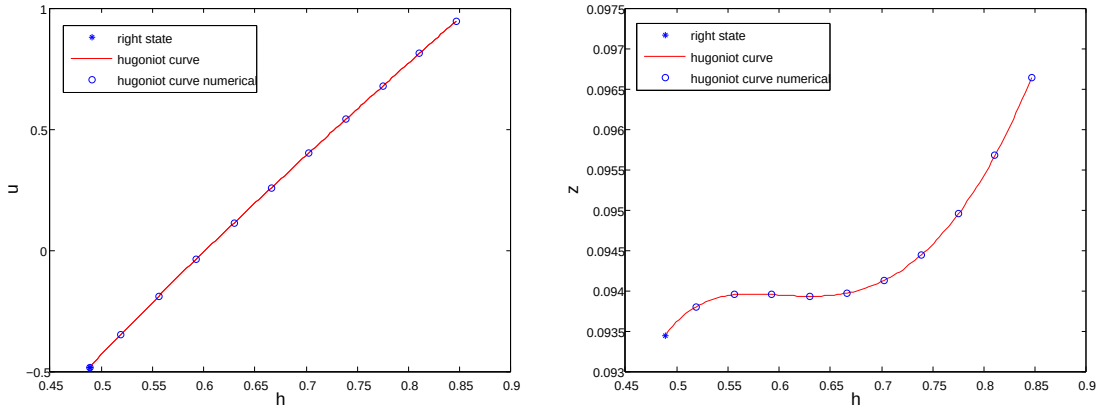

(a) (b)

Figure 17: Hugoniot curves for external shock

6.6 Hugoniot curves

This is designed to measure the convergence due to the numerical viscosity discussed in Section 1. We consider $c = 0$ and the Grass formula with $A = 0.1$. Consider a given right state $h_R = 4.8863763300885e-1$, $u_R = -4.8295086427435e-1$, $(z_b)_R = 9.3440819151415e-2$. Using the jump relations (3.22) we may compute the left states that can be connected by an entropy shock associated to the external velocity S_R. In order to numerically compute the Hugoniot curve given by the numerical scheme, we solve a family of Riemann problems whose initial conditions are given by the fixed right state and some of the left states lying on the exact Hugoniot curve. The 4W-HLLC is applied to these Riemann problems with $\Delta x = 0.001$. At time $t = 1$, the location of the shock is detected and the value of the left state is stored. In Fig. 17 the theoretical and numerical Hugoniot curves are composed.

Next a similar procedure has been applied to a Hugoniot curve corresponding to internal shocks, that is, entropy shocks associated to the second characteristic curve. In this case we fixed the left state $h_L = 1$, $u_L = 1$, $z_L = 1$. Fig. 18 shows the comparison at time $t = 1$ of the right states obtained from (3.22) and computed numerically with 4W-HLLC. In both cases a very good agreement is found.

7 2D test case

The scheme can be easily extended for the 2D case. We refer to [???] for further details.

Let us consider here a case of moving bottom. We shall consider the domain $D = [-1, 1] \times [-1, 1]$ and the initial condition

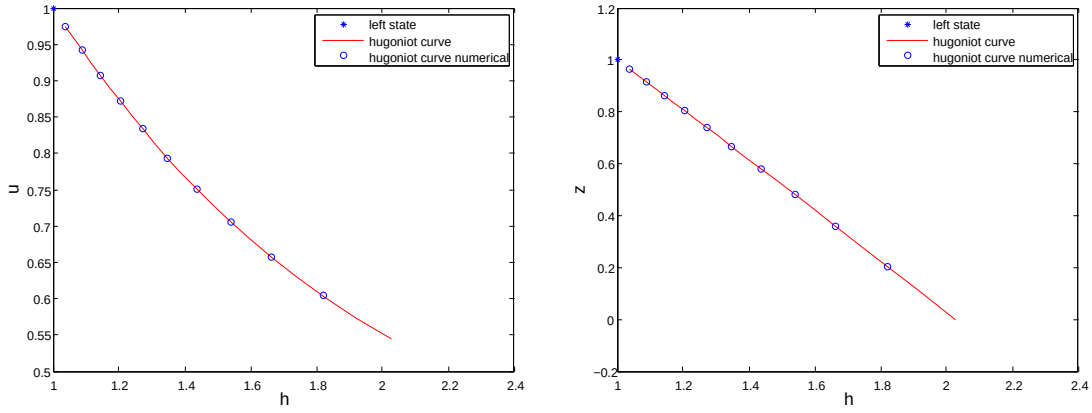

(a) (b)

Figure 18: Hugoniot curves for internal shock

$$z_b(\vec{x},0) = \begin{cases} 1.1 + 0.05\cos(10|\vec{x}|) & \text{if } |\vec{x}| \leq \pi/10, \\ 1.05 & \text{otherwise.} \end{cases} \tag{7.1}$$

$$h(\vec{x},0) + z_b(\vec{x},0) = 2, \quad q(\vec{x},0) = (1,0), \quad c(\vec{x},0) = 0; \tag{7.2}$$

for $\vec{x} \in [-1,1] \times [-1,1] \in \mathbb{R}^2$.

Then, we set the boundary conditions

$$\begin{aligned} q_y(\vec{x},t) &= 0, \quad \text{for } \vec{x} \in [-1,1] \times \{-1,1\},\ t \geq 0 \\ q_x(\vec{x},t) &= 1, \quad \text{for } \vec{x} \in -1 \times [-1,1],\ t \geq 0 \\ c_x(\vec{x},t) &= 0.02, \quad \text{for } \vec{x} \in -1 \times [-1,1],\ t \geq 0, \end{aligned} \tag{7.3}$$

where $q = (q_x, q_y)$ and we consider open boundary conditions for the remaining cases.

We consider 100 points in the x and y direction respectively and a second order extension is used (referencia ????)

Figures 19 to 21 show the results obtained with Roe, E3W-HLLC and 4W-HLLC. In general, we see a good agreement between the results. In general, the E3W-HLLC scheme is more difussive than the other two schemes, specially if we do not use a high-order reconstruction technique.

8 Conclusions

In this paper two HLLC solvers have been defined for the turbidity current model (2.8). The essentially three-wave HLLC solver preserves the non-negativity of the current thickness if $q_b = 0$. Under some assumptions on the form of q_b when $q_b \neq 0$,

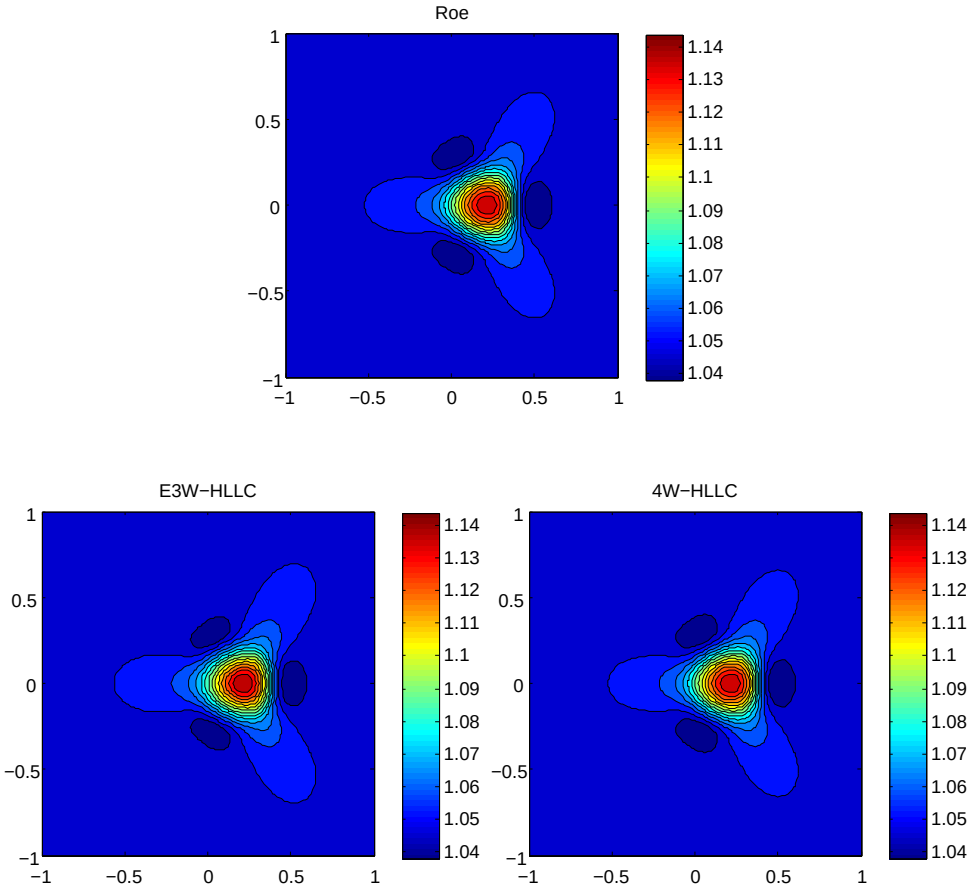

Figure 19: Topography elevation at time $t = 20$

the non-negativity of the layer of sediment is also ensured. Moreover, the three-wave HLLC solver for fixed flat topography is entropy satisfying as in that case it essentially coincides with Suliciu scheme presented in [3]. A four-wave HLLC is also defined and some conditions that ensures the positivity of h are also derived if $q_b = 0$. Both schemes give similar results, being the four-wave solver more accurate. Moreover, the results are close to those provided by the Roe scheme introduced in [18]. Concerning the efficiency, both HLLC solvers are cheaper than Roe as they do not need the eigenstructure of the system. In the simulations shown above, a speedup of about 60% is obtained for the four-wave HLLC solver.

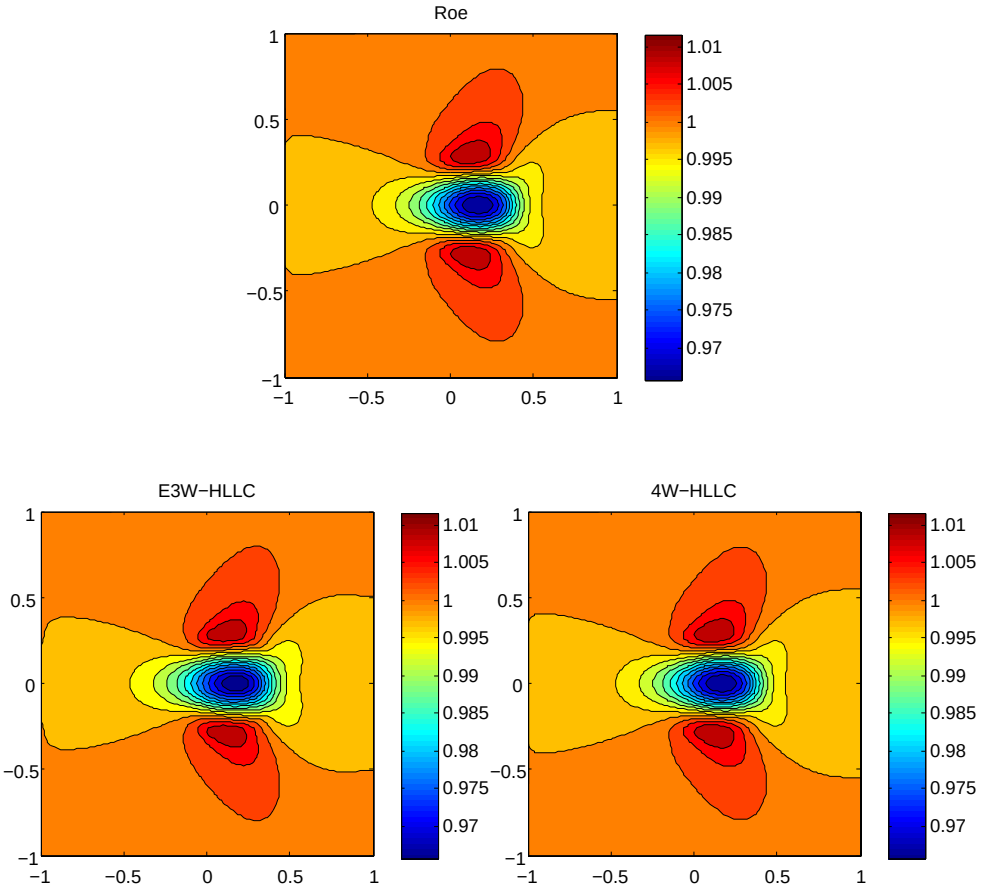

Figure 20: Discharge on the x direction at time $t = 20$

A Proof of Theorem 5.1

For the sake of completeness we give here the proof. First, let us remark that $p(h, c)$ defined by (5.8) verifies that

$$\forall h, c > 0, \quad \frac{\partial}{\partial h}\left(h\sqrt{\frac{\partial p}{\partial h}(h, c)}\right) > 0, \tag{A.1}$$

$$h\sqrt{\frac{\partial p}{\partial h}(h, c)} \to \infty \text{ as } h \to \infty, \tag{A.2}$$

$$\frac{\partial}{\partial h}\left(h\sqrt{\frac{\partial p}{\partial h}(h, c)}\right) \leq \alpha\sqrt{\frac{\partial p}{\partial h}(h, c)}, \tag{A.3}$$

where $\alpha = 3/2$.

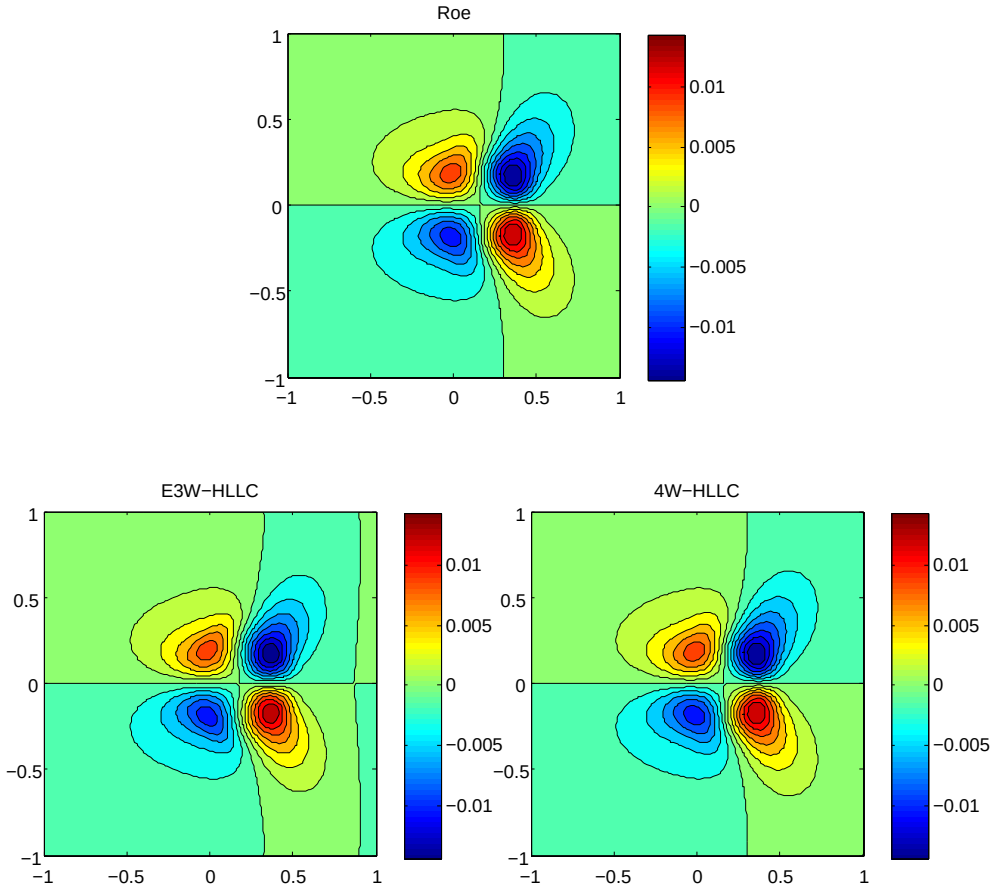

Figure 21: Discharge on the y direction at time $t = 20$

(A.1)-(A.2) allow us to define an inverse function $\psi(\cdot, c) : (0, \infty) \to (0, \infty)$ for each c,

$$h\sqrt{\frac{\partial p}{\partial h}(h, c)} = k \Leftrightarrow h = \psi(h, k). \tag{A.4}$$

Then, we have the following Lemma:

Lemma A.1 *Assume $k_R > 0$ and define*

$$\frac{k_L}{h_L} = \sqrt{\frac{\partial p}{\partial h}(h_L, c_L)} + \alpha \left(\frac{\mathcal{P}_{LR}}{k_R} + u_L - u_R \right)_+, \tag{A.5}$$

then

$$\frac{1}{h_L} + \frac{k_R(u_R - u_L) - \mathcal{P}_{LR}}{k_L(k_L + k_R)} \geq \frac{1}{\psi(k_L, c_L)}. \tag{A.6}$$

PROOF: Suppose first that

$$k_R(u_R - u_L) - \mathcal{P}_{LR} \geq 0, \tag{A.7}$$

then

$$k_L = h_L\sqrt{\frac{\partial p}{\partial h}(h_L, c_L)} \Leftrightarrow \psi(k_L, c_L) = h_L \tag{A.8}$$

and the result follows. Assume now

$$k_R(u_R - u_L) - \mathcal{P}_{LR} < 0, \tag{A.9}$$

and define

$$X = \frac{\mathcal{P}_{LR}}{k_R} + u_L - u_R > 0. \tag{A.10}$$

Then, (A.6) is equivalent to

$$1 - \frac{k_R}{k_L + k_R}\frac{X}{\sqrt{\frac{\partial p}{\partial h}(h_L, c_L)} + \alpha X} \geq \frac{h_L}{\psi(k_L, c_L)}. \tag{A.11}$$

Denote by

$$\theta = \frac{\sqrt{\frac{\partial p}{\partial h}(h_L, c_L)}}{\sqrt{\frac{\partial p}{\partial h}(h_L, c_L)} + \alpha X}, \quad 1 - \theta = \frac{\alpha X}{\sqrt{\frac{\partial p}{\partial h}(h_L, c_L)} + \alpha X}. \tag{A.12}$$

It is enough to prove

$$1 - \frac{1-\theta}{\alpha} - \frac{h_L}{\psi\left(h_L\left(\sqrt{\frac{\partial p}{\partial h}(h_L, s_L)} + \alpha X\right), c_L\right)} \geq 0. \tag{A.13}$$

From (A.3) we get

$$\frac{\partial \psi}{\partial k}(k, c) \geq \frac{\psi(k, c)}{\alpha k} \tag{A.14}$$

and

$$\frac{\partial}{\partial k}\left(\psi(k, c)k^{-1/\alpha}\right) \geq 0, \tag{A.15}$$

so that

$$\forall \lambda \geq 1, \quad \psi(\lambda k, c) \geq \lambda^{1/\alpha}\psi(k, c). \tag{A.16}$$

Thus, it is enough to prove

$$1 - \frac{1-\theta}{\alpha} - \theta^{1/\alpha} \geq 0, \tag{A.17}$$

and this is indeed the case when $0 < \theta \leq 1$ and $\alpha \geq 1$. □

Remark A.1 *The result of the lemma can be symmetrized and for any $k_L > 0$, the value*

$$\frac{k_R}{h_R} = \sqrt{\frac{\partial p}{\partial h}(h_R, c_R)} + \alpha \left(-\frac{\mathcal{P}_{LR}}{k_L} + u_L - u_R \right)_+, \tag{A.18}$$

satisfies

$$\frac{1}{h_R} + \frac{k_L(u_R - u_L) + \mathcal{P}_{LR}}{k_R(k_L + k_R)} \geq \frac{1}{\psi(k_R, c_R)}. \tag{A.19}$$

PROOF: [Theorem 5.1]

Let us assume that $\mathcal{P}_{LR} > 0$, being the other case completely analogous.

Then, by Remark A.1 we have

$$\frac{1}{h_R} + \frac{k_L(u_R - u_L) + \mathcal{P}_{LR}}{k_R(k_L + k_R)} \geq \frac{1}{\psi(k_R, c_R)}. \tag{A.20}$$

Now, if $k_R(u_R - u_L) - \mathcal{P}_{LR} \geq 0$, then

$$\frac{1}{h_L} + \frac{k_R(u_R - u_L) - \mathcal{P}_{LR}}{k_L(k_L + k_R)} \geq \frac{1}{h_L} \geq \frac{1}{\psi(k_L, c_L)}. \tag{A.21}$$

If $k_R(u_R - u_L) - \mathcal{P}_{LR} < 0$, then

$$k_R \geq h_R \sqrt{\frac{\partial p}{\partial h}(h_R, c_R)} \text{ and } \mathcal{P}_{LR} \geq 0 \tag{A.22}$$

and we have $k_L \geq \widehat{k}_L$ with

$$\frac{\widehat{k}_L}{h_L} = \sqrt{\frac{\partial p}{\partial h}(h_L, c_L)} + \alpha \left(\frac{\mathcal{P}_{LR}}{k_R} + u_L - u_R \right)_+. \tag{A.23}$$

By applying Lemma A.1 to the pair $(\widehat{k}_L, k_R)$ we have

$$\frac{1}{h_L} + \frac{k_R(u_R - u_L) - \mathcal{P}_{LR}}{\widehat{k}_L(\widehat{k}_L + k_R)} \geq \frac{1}{\psi(\widehat{k}_L, c_L)}, \tag{A.24}$$

and by using the fact that $k_R(u_R - u_L) - \mathcal{P}_{LR} < 0$ and that $f(k) = -1/(k(k + k_R))$ is an increasing function of $k \in (0, \infty)$ we obtain

$$\frac{1}{h_L} + \frac{k_R(u_R - u_L) - \mathcal{P}_{LR}}{k_L(k_L + k_R)} \geq$$
$$\frac{1}{h_L} + \frac{k_R(u_R - u_L) - \mathcal{P}_{LR}}{\widehat{k}_L(\widehat{k}_L + k_R)} \geq \frac{1}{\psi(\widehat{k}_L, c_L)} \geq \frac{1}{\psi(k_L, c_L)}. \tag{A.25}$$

□

Remark A.2 *We have actually proved that*

$$\begin{array}{l} \dfrac{1}{h_L}+\dfrac{k_R(u_R-u_L)-\mathcal{P}_{LR}}{k_L(k_L+k_R)} \geq \dfrac{1}{\psi(k_L,c_L)}, \\ \dfrac{1}{h_R}+\dfrac{k_L(u_R-u_L)+\mathcal{P}_{LR}}{k_R(k_L+k_R)} \geq \dfrac{1}{\psi(k_R,c_R)}, \end{array} \tag{A.26}$$

which can be used to show that the numerical scheme for fixed flat topography is entropy satisfying.

B Definition of a four-wave HLLC solver

We consider now the system given by (5.1)-(a) and the following modification of (5.1)-(b):

$$\left\{ \begin{array}{lcl} S_L(z_{bL}^M - z_{bL}) & = & (z_{bL}^M \tilde{q}_{bL}^M - z_{bL}\tilde{q}_{bL}), \\ S_R(z_{bR} - z_{bR}^*) & = & (z_{bR}\tilde{q}_{bR} - z_{bR}^*\tilde{q}_{bR}^*), \\ S_L(z_{bL}^M - z_{bL}) + S_M(z_{bL}^* - z_{bL}^M) & & \\ \quad +S^*(z_{bR}^* - z_{bL}^*) + S_R(z_{bR} - z_{bR}^*) & = & (z_{bR}\tilde{q}_{bR} - z_{bL}\tilde{q}_{bL}). \end{array} \right. \tag{B.1}$$

Now, system (5.1)-(a)-(B.1) can be solved by considering h_L^M and S_M as two free parameters:

$$c_R^* = c_R, \quad c_L^* = c_L, \quad c_L^M = c_L,$$

$$S^* = \frac{S_M(h_L(S_L-u_L)-S_Lh_L^M)+h_Ru_R(S_R-u_R)+h_L(u_L^2-S_L^2)+S_L^2h_L^M-\mathcal{P}_{LR}}{h_R(S_R-u_R)+h_L(u_L-S_L)+(S_L-S_M)h_L^M}, \tag{B.2}$$

$$u_L^* = u_R^* = S^*, \tag{B.3}$$

$$u_L^M = \frac{h_Lu_L+S_L(h_L^M-h_L)}{h_L^M}, \tag{B.4}$$

$$h_L^* = \frac{h_L(u_L-S_L)+(S_L-S_M)h_L^M}{S^*-S_M}, \tag{B.5}$$

$$h_R^* = \frac{h_R(u_R-S_R)}{S^*-S_R}, \tag{B.6}$$

$$z_{bL}^M = \frac{z_{bL}(-S_L+\tilde{q}_{bL})}{\tilde{q}_{bL}^M-S_L}, \quad z_{bR}^* = \frac{z_{bR}(S_R-\tilde{q}_{bR})}{S_R-\tilde{q}_{bR}^*}, \tag{B.7}$$

$$z_{bL}^* = \frac{S_L(z_{bL}-z_{bL}^M)+S_R(z_{bR}^*-z_{bR})+z_{bR}\tilde{q}_{bR}-z_{bL}\tilde{q}_{bL}+S_Mz_{bL}^M-S^*z_{bR}^*}{S_M-S^*}, \tag{B.8}$$

$$\mathcal{P}_{LR} = F_P(W_R)_{[2]} - F_P(W_L)_{[2]} + \mathcal{B}(W_L,W_R)_{[2]}. \tag{B.9}$$

Finally, to fully define the scheme, h_L^M and S_M must be defined:

Definition of h_L^M:

- In order to preserve water at rest solutions, we define h_L^M as follows:

$$h_L^M = h_L^* + z_{bR} - z_{bL}. \tag{B.10}$$

In this particular case, expressions (B.2) to (B.8) can be simplified. For instance, from (B.5) we get

$$h_L^* = \frac{h_L(u_L - S_L) + (S_L - S_M)(z_{bR} - z_{bL})}{S^* - S_M} + \frac{S_L - S_M}{S^* - S_M} h_L^*, \tag{B.11}$$

and thus

$$h_L^* = \frac{h_L(u_L - S_L) + (S_L - S_M)(z_{bR} - z_{bL})}{S^* - S_L}. \tag{B.12}$$

From (B.2) we have

$$\begin{aligned} S^*(h_R(S_R - u_R) + h_L(u_L - S_L)) + (S_L - S_M)(S^* - S_L)h_L^M \\ = S_M h_L(S_L - u_L) + h_R u_R(S_R - u_R) + h_L(u_L^2 - S_L^2) - \mathcal{P}_{LR}, \end{aligned} \tag{B.13}$$

and using the fact that

$$\begin{aligned} &(S_L - S_M)(S^* - S_L)h_L^M \\ &= (S_L - S_M)\left(h_L(u_L - S_L) + (S_L - S_M)(z_{bR} - z_{bL}) + (S^* - S_L)(z_{bR} - z_{bL})\right) \\ &= (S_L - S_M)h_L(u_L - S_L) + (S_L - S_M)(S^* - S_M)(z_{bR} - z_{bL}), \end{aligned} \tag{B.14}$$

some easy calculations show that

$$S^* = \frac{h_R u_R(S_R - u_R) + h_L u_L(u_L - S_L) + S_M(S_L - S_M)(z_{bR} - z_{bL}) - \mathcal{P}_{LR}}{h_R(S_R - u_R) + h_L(u_L - S_L) + (S_L - S_M)(z_{bR} - z_{bL})}. \tag{B.15}$$

- If $\widetilde{q_b} = 0$, a more general family of stationary solutions is given by:

$$q = constant, c = constant, \frac{u^2}{2} + g(1 + Rc)(h + z_b) = constant.$$

In order to preserve this more general family, a better choice for h_L^M would be given by:

$$\mathcal{E}(W_L^M) = \mathcal{E}(W_L^*), \tag{B.16}$$

where

$$\mathcal{E}(W) = \frac{u^2}{2} + g(1 + Rc)(h + z_b).$$

Nevertheless, we have not been able to find an analytical expression of the solution of the system (5.1)-(a), (B.1), (B.16). An iterative procedure could be used to approximate the solution, but in this article we have only considered the simplest choice (B.10).

Definition of S^M:

Let us now discuss, some possible definitions for S_M.

- *Steady bottom*: If $q_b = 0$, we choose

$$S_M = 0. \tag{B.17}$$

- *Moving bottom*: In this case, S_M is approximated by the corresponding eigenvalue of $\mathcal{A}(W)$ in an given intermediate state.

Remark B.1 *If $\tilde{q}_b = 0$ and the bottom is flat then, the essentially three-wave and the four-wave HLLC solver coincide. The main difference between both solvers is that, in the four-wave one, S_M explicitly appears in the definition of the hydrodynamic variables.*

Concerning the positivity-preserving property of the four-wave HLLC, if $\tilde{q}_b = 0$, the following result can be shown:

Proposition B.1 *Assume that $S_L < S_M = 0 < S^*$ and*

$$0 < h_L^M \leq \max\left(\frac{h_L(S_L - u_L)}{s_L}, \right.$$
$$\left. \frac{h_R(u_R - S_R)^2 + h_L(u_L - S_L)^2 + h_L u_L(S_R + 2S_L - 2u_L) - h_L S_L S_R - \mathcal{P}_{LR}}{-S_L(S_R - S_L)}\right). \tag{B.18}$$

Then, the HLLC scheme is positive and well defined, that is, if $h_L \geq 0$ and $h_R \geq 0$, then $h_L^* \geq 0$, $h_R^* \geq 0$ and $S^* < S_R$.

Proof:

From (B.5), we have

$$h_L^* = \frac{h_L(u_L - S_L) + S_L h_L^M}{S^*}, \tag{B.19}$$

which is positive by the first upper bound in (B.18).

Then, from (B.6) we have

$$h_R^* = \frac{h_R(u_R - S_R)}{S^* - S_R}, \tag{B.20}$$

which is positive as long as $u_R - S_R \leq 0$ and $S^* \leq S_R$.

On the one hand, we may define $S_L = u_L - \dfrac{k_L}{h_L}$ and $S_R = u_R + \dfrac{k_R}{h_R}$ as it was done in Theorem 5.1.

On the other hand,

$$\begin{aligned} & S^* - S_R \\ &= \frac{h_R u_R(S_R - u_R) + h_L(u_L^2 - S_L^2) + S_L^2 h_L^M - \mathcal{P}_{LR} - S_R(h_R(S_R - u_R) + h_L(u_L - S_L) + S_L h_L^M)}{h_R(S_R - u_R) + h_L(u_L - S_L) + S_L h_L^M} \\ &= \frac{h_R(u_R S_R - u_R^2 - S_R^2 + S_R u_R) + h_L(u_L^2 - S_L^2 - S_R u_L + S_R S_L) + S_L(S_L - S_R)h_L^M - \mathcal{P}_{LR}}{h_R(S_R - u_R) + h_L(u_L - S_L) + S_L h_L^M}. \end{aligned} \tag{B.21}$$

Now remark that

$$\frac{h_R(S_R - u_R) + h_L(u_L - S_L)}{-S_L} \geq \frac{h_L(u_L - S_L)}{-S_L} \geq h_L^M, \tag{B.22}$$

which means that $S^* - S_R \leq 0$ as long as the numerator in the right hand side of (B.21) is non positive.

Some easy calculations show that this is the case when

$$h_L^M \leq \frac{h_R(u_R - S_R)^2 + h_L(u_L - S_L)^2 + h_L u_L(S_R + 2S_L - 2u_L) - h_L S_L S_R - \mathcal{P}_{LR}}{-S_L(S_R - S_L)} \tag{B.23}$$

which completes the proof.

□

Remark B.2 *In general, the difficulty in (B.18) is to prove that the upper bound is positive. In fact, this is not possible when 'big steps' are present in the bottom. In those cases, the essentially three-wave HLLC scheme should be used to ensure the non-negativity.*

Finally, let us check the well-balanced property of the numerical scheme given by this HLLC-solver. Given two states $W_L = [h_L, 0, c_L h_L, z_{b\,L}]^T$, $W_R = [h_R, 0, c_R h_R, z_{b\,R}]^T$ such that:

$$c_L = c_R = \bar{c}, \quad h_L + z_{b\,L} = h_R + z_{b\,R},$$

from definitions (B.2)- (B.8), (B.12) and (B.15) one can check the following equalities:

$$S_M = S^* = 0, \quad W_L^* = W_R^* = W_R, \quad W_L^M = W_L,$$

and the result follows.

References

[1] R. Abgrall and S. Karni. A comment on the computation of non-conservative products. *Journal of Computational Physics*, 229(8):2759–2763, Apr. 2010.

[2] M. Altinaker, W. Graf, and E. Hopfinger. Flow structure in turbidity currents. *Journal of Hydraulic Research*, 34(5), 1996.

[3] F. Bouchut. *Nonlinear stability of finite volume methods for hyperbolic conservation laws and well-balanced schemes for sources.* Frontiers in Mathematics. Birkhäuser Verlag, Basel, 2004.

[4] S. F. Bradford and N. D. Katopodes. Hydrodynamics of turbid underflows. i: Formulation and numerical analysis. *Journal of Hydraulic Engineering*, 125(10):1006–1015, 1999.

[5] M. J. Castro, P. G. LeFloch, M. L. Muñoz-Ruiz, and C. Parés. Why many theories of shock waves are necessary: Convergence error in formally path-consistent schemes. *Journal of Computational Physics*, 227(17):8107–8129, Sept. 2008.

[6] M. Castro Díaz, E. Fernández-Nieto, and A. Ferreiro. Sediment transport models in shallow water equations and numerical approach by high order finite volume methods. *Computers & Fluids*, 37(3):299–316, Mar. 2008.

[7] S. Cordier, M. Le, and T. Morales de Luna. Bedload transport in shallow water models: Why splitting (may) fail, how hyperbolicity (can) help. *Advances in Water Resources*, 34(8):980–989, Aug. 2011.

[8] G. Dal Maso, P. G. Lefloch, and F. Murat. Definition and weak stability of nonconservative products. *J. Math. Pures Appl. (9)*, 74(6):483–548, 1995.

[9] A. C. Fowler, N. Kopteva, and C. Oakley. The formation of river channels. *SIAM Journal on Applied Mathematics*, 67(4):1016–1040, 2007.

[10] A. Grass. Sediment transport by waves and currents. *SERC London Cent. Mar. Technol*, Report No. FL29, 1981.

[11] A. Harten, P. D. Lax, and B. van Leer. On upstream differencing and godunov-type schemes for hyperbolic conservation laws. *Siam Review*, 25, 1983.

[12] T. Y. Hou and P. G. Le Floch. Why nonconservative schemes converge to wrong solutions: error analysis. *Math. Comput.*, 62(206):497–530, Apr. 1994.

[13] S. M. Khan, J. Imran, S. Bradford, and J. Syvitski. Numerical modeling of hyperpycnal plume. *Marine Geology*, 222-223:193–211, November 2005.

[14] Y. Kubo. Experimental and numerical study of topographic effects on deposition from two-dimensional, particle-driven density currents. *Sedimentary Geology*, 164(3-4):311–326, February 2004.

[15] Y. Kubo and T. Nakajima. Laboratory experiments and numerical simulation of sediment-wave formation by turbidity currents. *Marine Geology*, 192(1-3):105–121, December 2002.

[16] D. A. Lyn and M. Altinakar. St. Venant–Exner equations for Near-Critical and transcritical flows. *Journal of Hydraulic Engineering*, 128(6):579–587, June 2002.

[17] T. Morales de Luna, M. J. Castro Díaz, and C. Parés Madroñal. A duality method for sediment transport based on a modified Meyer-Peter & Müller model. *Journal of Scientific Computing*, 48:258–273, Dec. 2010.

[18] T. Morales de Luna, M. J. Castro Díaz, C. Parés Madroñal, and E. D. Fernández Nieto. On a shallow water model for the simulation of turbidity currents. *Communications in Computational Physics*, 6(4):848–882, 2009.

[19] P. H. Morris and D. J. Williams. Relative celerities of mobile bed flows with finite solids concentrations. *Journal of Hydraulic Engineering*, 122(6):311–315, June 1996.

[20] M. L. Muñoz Ruiz and C. Parés. On the convergence and Well-Balanced property ofPath-Conservative numerical schemes for systems ofbalance laws. *Journal of Scientific Computing*, 48(1-3):274–295, Oct. 2011.

[21] C. Parés. Numerical methods for nonconservative hyperbolic systems: a theoretical framework. *SIAM J. Numer. Anal.*, 44(1):300–321 (electronic), 2006.

[22] C. Parés and M. Castro. On the well-balance property of Roe's method for nonconservative hyperbolic systems. Applications to shallow-water systems. *M2AN Math. Model. Numer. Anal.*, 38(5):821–852, 2004.

[23] C. Parés and M. L. Muñoz Ruiz. On some difficulties of the numerical approximation of nonconservative hyperbolic systems. *Bol. Soc. Esp. Mat. Apl.*, 47(47):23–52, July 2009.

[24] G. Parker, Y. Fukushima, and H. M. Pantin. Self-accelerating turbidity currents. *Journal of Fluid Mechanics*, 171:145–181, 1986.

[25] E. F. Toro. *Shock-capturing methods for free-surface shallow flows*. John Wiley, Mar. 2001.

[26] E. F. Toro, M. Spruce, and W. Speares. Restoration of the contact surface in the HLL-Riemann solver. *Shock Waves*, 4(1):25–34, July 1994.